Politecnico di Torino

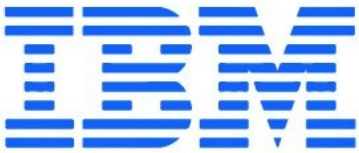

Politecnico di Torino - IBM Research Zürich

Master Degree in Nanotechnologies for ICT

a.a. 2025/2026

Solving combinatorial optimization problems with coupled VO_2 oscillators

Relatori:

Dr. Siegfried Karg
Prof. Carlo Ricciardi
Dr. Valeria Bragaglia
Dr. Wooseok Choi

Candidato:

Tommaso Negrini

Dedicato alla mia bisnonna Florinda (Flora) Fulda.

Acknowledgements

I would like to express my deep gratitude to Dr. Siegfried (Sigi) Karg, my local supervisor at IBM Research. His availability and guidance through all eight months of my permanence at the Research Labs has helped me a lot during this unforgettable experience. I still remember with a smile your expression: "It is not rocket science" when we had to deal with some tasks during the project and i also appreciated our extra-thesis talks, whether it was in your office, in the experimental lab or during lunch time.

Many thanks to Dr. Valeria Bragaglia who has given me valuable suggestions during the meetings and provided me continuous feedback along the path.

I thank Prof. Carlo Ricciardi, my supervisor at Politecnico di Torino who coordinated me from Italy and, together with Dr. Bragaglia, has allowed me to have the first interaction with IBM Research and the opportunity to find an available position for the Master project.

Thanks to Dr. Wooseok Choi, which i had the opportunity to work with and who provided help and organization with the project on the resistive RAM side.

I wish to thank also Dr. Berndt Gotsmann, manager of the Physics and Science of Information (PSI) group which i had the privilege of being part of, who gave me important feedback especially during the weekly presentations.

I enjoyed a lot the time spent with the members of the PSI and Neuromorphic Devices and Systems Group, having the opportunity to meet friendly and interesting people. I felt really comfortable and I appreciated all the activities organized outside from work. My deep appreciation goes to all of you.

Sincere thanks to all the members of the BRNC facility, whose expertise and resources have made possible the realization of the vanadium dioxide chips used for the experiments and from which i learned a lot.

My thanks also go to my friends; i enjoyed our remote night calls even if we were not physically in the same place.

Last but not least, I am deeply thankful to my family which was always close to me every day from Italy and that gave the necessary presence to accompany me through this memorable journey.

Thank you, wish you all the best,
Tommaso

Table of Contents

List of Figures VIII

1 Introduction 1
1.1 Thesis organization/Motivation 1

2 Background 2
2.1 Neuromorphic computing and ONN 2
2.2 Combinatorial optimization problems 3
2.2.1 Maximum cut problem 3
2.2.2 Ising model 3
2.3 Vanadium dioxide-based oscillators 5
2.3.1 VO_2 as phase change material 5
2.3.2 Coupled VO_2 oscillators 6

3 Methodology used 7
3.1 VO_2 chip fabrication 7
3.1.1 Slow Thermal Annealing 7
3.1.2 VO_2 patterning 8
3.1.3 Top electrodes pattern definition 8
3.1.4 Metal evaporation 8
3.1.5 Wire bonding on Printed Circuit Board (PCB) 9
3.2 Experimental setup 11
3.3 Coupling schematics 16
3.3.1 Two coupled oscillators 16
3.3.2 Coupled network of more than two oscillators 17
3.4 ReRAM as coupling element 22
3.4.1 Programming ReRAM state 22
3.4.2 ReRAM integration 23
3.5 Analog phase tuning 24
3.5.1 Resistive analog phase tuning 24
3.6 Spice simulation of coupled oscillators 26

4 Experimental outcomes 27
4.1 Vanadium-dioxide oscillator characteristic 27
4.2 Capacitive and resistive coupling 30
4.2.1 Purely capacitive coupling 30
4.2.2 Purely resistive coupling 31
4.3 Four coupled oscillators network for Maxcut optimization 33
4.4 ReRAM coupling 37
4.5 Resistive analog phase tuning 38
4.5.1 Experimental results 38
4.6 Spice simulation results 41

5 Discussion over results 43
5.1 Two coupled oscillators 43
5.1.1 Capacitive coupling 43
5.1.2 Resistive coupling 43
5.2 Maxcut problem optimization through different coupling schemes . 45
5.3 Analog phase tuning 47

6 Summary 48

Bibliography 50

List of Figures

2.1 From the connected graph to the vanadium dioxide network. Weights are stored in a weight matrix; after initialization of the system, it is driven into ground state where a fixed phase relationship between oscillators is defined. Figure taken from[6] 4

3.1 Left: An inset of the wire bonded VO_2 chip. Right: Inside the cryostat chamber: PCB mounted on cryostat holder 9
3.2 Process flow illustrating steps for the fabrication of the VO_2 chip . . 10
3.3 Picture showing the cryostat apparatus 11
3.4 Two breadboards where the coupling circuit is implemented 12
3.5 LabView output window 13
3.6 LabView control window 13
3.7 Triangular shaped supply voltage (red signal) used to trigger oscillation on a VO_2 device (green signal) 14
3.8 Trapezoidal shape supply voltage (red signal) used to drive oscillations (green signal) 14
3.9 Electrical schematic of two capacitively coupled (via capacitance C_c) VO_2 oscillators 16
3.10 Electrical schematic of two resistively coupled (via resistor R_c) VO_2 oscillators 17
3.11 Maximum cut optimization for two graphs: nodes are grouped into two partitions (black and white) and the red line shows the cut . . 18
3.12 Pure capacitive coupling of the connected graphs used for Maxcut optimization 18
3.13 Two VO_2 oscillators coupled via a transistor, a resistance and a capacitance 19
3.14 Coupling circuit of figure 3.14 applied to the two connected graphs . 19
3.15 Two VO_2 oscillators coupled via a series resistance R_c, a resistance R which models the dummy ReRAM and a capacitance C. In this experiment, the voltage drop across R is measured 20

3.16 Coupling circuit schematic similar to the one presented in figure 3.16 except for the addition of a transistor. Together with R, it models the dummy 1T1R cell 21
3.17 Left: 1T1R chip. Right: Schematic of the 1T1R array 22
3.18 Connected graphs with the 1T1R chip integrated in the coupling circuit 23
3.19 Schematic of the coupling circuit used for analog phase tuning experiment 25
3.20 Left: Spice screenshot of two coupled VO_2 oscillator. Right: Spice screenshot of a single oscillator (Maffezzoni model in the yellow box) with the feedback circuit 26

4.1 Hysteresis curves representing the IV characteristic for a single VO_2 oscillator. Red and blue curves were obtained respectively at 251° K and 268° K 27
4.2 Effect of the feedback resistance on the hysteretic IV curve: a load line is generated and it intercepts the characteristic in two points that happen to be the metallic and insulating state of Vanadium dioxide. Figure taken from[6] 28
4.3 Left: Oscillating voltage of two uncoupled oscillators. Right: Inset of the voltage profile, dashed curves are the supply voltages while solid curves represent the output periodic voltages. No frequency synchronization is observed 30
4.4 Left: Oscillating voltage of two oscillators coupled with a capacitor. Right: Inset of the voltage profile, dashed curves are the supply voltages while solid curves represent the output periodic voltages. . 31
4.5 Left: Output voltage of two oscillators coupled with a 10 kΩ resistance. Right: Inset of the voltage profile 31
4.6 Left: Output voltage of two oscillators coupled with a 30 kΩ resistance. Right: Inset of the voltage profile 32
4.7 Left: Output voltage of two oscillators coupled with a 40 kΩ resistance. Right: Inset of the voltage profile 32
4.8 Left: Output voltage of two oscillators coupled with a 50 kΩ resistance. Right: Inset of the voltage profile 32
4.9 Left: Oscillating voltage for the square Maxcut configuration Right: Inset of the voltage profile 33
4.10 Left: Oscillating voltage for the 3 vs 1 Maxcut configuration Right: Inset of the voltage profile 33
4.11 Left: Oscillating voltage for the square Maxcut configuration Right: Inset of the voltage profile 34

4.12 Left: Oscillating voltage for the square Maxcut configuration Right: Inset of the voltage profile 34
4.13 Left: A zoom of the oscillating voltage for the square Maxcut configuration Right: Voltage drop measured across coupling resistances R_i with i=1,2,3,4 representing the branch in the graph 35
4.14 Left: A zoom of the oscillating voltage for the 3 vs 1 Maxcut configuration Right: Voltage drop measured across coupling resistances R_i with i=1,2,3,4 representing the branch in the graph 35
4.15 Left: A zoom of the oscillating voltage for the square Maxcut configuration Right: Voltage drop measured across coupling resistances R_i with i=1,2,3,4 representing the branch in the graph 36
4.16 Left: A zoom of the oscillating voltage for the 3 vs 1 Maxcut configuration Right: Voltage drop measured across coupling resistances R_i with i=1,2,3,4 representing the branch in the graph 36
4.17 Left: A zoom of the oscillating voltage profile of four oscillators coupled in the square configuration. The coupling circuit comprises LRS 1T1R devices. Right: Fast Fourier Transform (FFT) plot of the oscillating system 37
4.18 Left: A zoom of the oscillating voltage profile of four oscillators coupled in the 3 vs 1 configuration. The coupling circuit comprises LRS 1T1R devices. Right: FFT plot of the oscillating system . . . 37
4.19 Right: FFT plot of the two coupled oscillators with 100 pF capacitor and 1 kΩ resistance. Left: Polar graph which highlights the phase delay between the two oscillators 38
4.20 Right: FFT plot of the two coupled oscillators with 100 pF capacitor and 10 kΩ resistance. Left: Polar graph which shows the phase delay 39
4.21 Right: FFT plot of the two coupled oscillators with 100 pF capacitor and 20 kΩ resistance. Left: Phase delay polar graph 39
4.22 Right: FFT plot of the two coupled oscillators with 100 pF capacitor and 30 kΩ resistance. Left: Phase delay polar graph 39
4.23 Right: Average phase delay with standard deviation measured for each coupling resistance in the specified range on the x-axis. The operating temperature is 225° K. Left: Same graph obtained at the temperature of 250° K 40
4.24 Right: Average phase delay with standard deviation measured for each coupling resistance at the operating temperature of 270° K. Left: All previous curves overlapped in the same graph. 40
4.25 Left: Oscillating voltage profile for the Spice model VO_2 device (blue curve) and for the experimental one (red curve). Right: An inset of the oscillating voltage from the figure on the left. 41

4.26 Left: In-phase behavior of two coupled oscillators in Spice simulator. The output voltages appear totally overlapped when the coupling resistance is 2 kΩ. The flat light blue curve stands for the voltage drop across the coupling resistance. Right: Out-of-phase coupling of the devices when the coupling resistance is set to 30 kΩ. Below, the voltage drop which is limited in the interval (-0.5,0.5) V. 42

Chapter 1

Introduction

1.1 Thesis organization/Motivation

The goal of the present thesis is to implement a circuital solution to couple electrical oscillators based on a phase change material, namely vanadium dioxide. Vanadium dioxide oscillators are able to exchange electrical energy between them by means of the coupling circuit. This is enough to ensure a phase synchronization of the oscillators which corresponds to a dynamical equilibrium position for the system. In this way, the oscillating system can behave as a neural network suited for solving simple combinatorial optimization problems. The computing information is encoded in a time delay between oscillators output waveforms, hence it is independent from voltage scaling or device scaling factors.

The structure of the thesis is briefly outlined herein. The background part presents the "big picture" around which the thesis orbits. It quickly describes new computing approaches such as Neuromorphic computing and Artificial Neural Networks (ANN), focusing on the subclass of Oscillating Neural Networks (ONN). An introduction regarding vanadium dioxide material and the special application of relaxation oscillator is given as a potential solution to implement ONN. The third chapter covers the details of the technological methods used to implement the experimental setup together with a description of the fabrication steps for the vanadium dioxide oscillators chip manufacturing. The different coupling circuit solutions are also given. The fourth chapter follows the same structure as the previous one by illustrating graphs and figures for each experimental test conducted, i.e. for each coupling circuit scheme anticipated in the previous chapter. An elucidation over the results and a further discussion on the adopted strategies is explained in the fifth chapter. The last (sixth) chapter is devoted to summarize the work.

Chapter 2

Background

2.1 Neuromorphic computing and ONN

In the last decade, the well known and extensively cited Moore's law has dealt with its end many times and, indeed, the scaling era of micro and nanoelectronics has slowed down, trying new roads to follow and new paradigms to adopt. The rise of AI, the deluge of unstructured data and the continuous high demand for problems optimization together with the important requirements of low power consumption and high speed of computation has led research flowing into novel computing paradigms such as Neuromorphic and In-memory computing. One such hardware that could serve as a platform for Neuromorphic computing is represented by Artificial Neural Networks (ANN) and, more specifically, taking into account the topic of this thesis, a subclass of ANN, namely Oscillating Neural Networks (ONN), have gained remarkable interest. The driving idea behind Neuromorphic computing approach is to have a biological brain-like behavior to solve problem harnessing the parallel computation capability of neurons, low processing time and low power consumption. In the case of an ONN, a network of interconnected nodes forms a graph: the graph nodes are oscillating devices that mimic the biological neurons whilst graph branches between nodes represent synaptic weights and set the strength of the interaction between nodes. One important characteristic typical of ONNs is the way computing information is generated in the network: rather than storing a charge or measuring the amplitude of an output signal, ONN information is encoded in the time delay existing between two computing units, i.e., two oscillating nodes. Having a signal living in the time domain makes the system robust to scaled power voltage supplies. Nowadays, the state of the art for ONN hardware is represented by CMOS-based Silicon ring oscillators. Although the outstanding performance makes this technology superior to others, it suffers from a major drawback, that is, scalability issues.

2.2 Combinatorial optimization problems

Computing deals with problem solving: from massive data analysis in finance market or climate models to molecular dynamics, from pattern recognition tasks to image and graphics generation. Hence, depending on the class of problem we want to solve, different algorithms are required and can be implemented. In computational theory, problems are divided into two main classes: decision problems and optimization problems (OP). The first class represents all those problems that can be posed as a yes/no answer[1]. The second, comprises tasks that deal with the search of the best solution from a set of feasible options. Usually, optimization problems are represented through an objective function that is subject to constraints and has to be minimized or maximized[2]. It is always desirable to organize an optimization problem into a decision-like form since it appears easier to solve and becomes possible to develop an algorithm for the resolution. On the other hand, optimization problems are not solvable via algorithms but they can be attacked through heuristic approaches or approximation routines that tend to minimize an error function. The motivation for solving optimization problems rely on the fact that many tasks belonging to different fields can be modeled as an optimization task; among many we find resources allocation, airline network optimization, Earth science problems, cybersecurity, etc[2]. In particular, a subset of OP called Combinatorial OP (COP) can be defined whenever the set of feasible solution is a finite discrete one. COPs are used in several applications like drug synthesis, resource allocation, computer vision and circuit layout design[3]

2.2.1 Maximum cut problem

Maximum cut (Maxcut) belongs to the class of COPs and, more specifically, is part of the Non Deterministic Polynomial Type problems (NP problems). The problem formulation is the following: given a graph, find a subset of the vertex set such that the number of edges between S and the complementary subset is as large as possible[4]. From a computational complexity standpoint, Maxcut is an NP-complete problem, hence not solvable in polynomial time by a deterministic algorithm. Knowing that, it is intractable to solve this kind of problem with traditional computing machines as the required power and time would be not sustainable. An efficient way to implement a Maxcut solver is through the aid of Ising machines, which will be presented in the next subsection.

2.2.2 Ising model

The Ising model is a mathematical approach, proposed by the German physicist Ernst Ising in 1920, to describe the formation of magnetic domains in ferroelectric

materials[5]. To be more precise, the Ising model describes what is known as a spin glass system, i.e. a magnetic environment characterized by a randomness in the arrangement of magnetic spins. Those magnetic domains interact with each other and with an external applied field contributing to the total energy Hamiltonian of the system. After writing down the expression for the Hamiltonian

$$H = \sum_{1<=i<=j<=n} J_{\mathrm{ij}} \cdot s_{\mathrm{i}} \cdot s_{\mathrm{j}} - \sum_{i=1}^{n} h_{\mathrm{i}} \cdot s_{\mathrm{i}}$$

it is possible to distinguish between the first term on the right-hand side that represents the domain interaction term, given by the summation of products $J_{\mathrm{ij}} \cdot s_{\mathrm{i}} \cdot s_{\mathrm{j}}$, and the second term that shows the influence of an external magnetic field on the magnetic moments. CO problems such as MaxCut can be efficiently modeled into a spin glass system and, leveraging the analogy between oscillating nodes in the ONN and Magnetic spins in the ferromagnetic domains, it can directly be mapped into an oscillating network and optimized through the natural evolution of the system toward ground state. Optimizing the COP means reaching the ground state for the ONN that, in turn, corresponds to the minimization of the Hamiltonian of the Ising model. That is, the solution of the problem is driven by the natural physical evolution of the ONN.

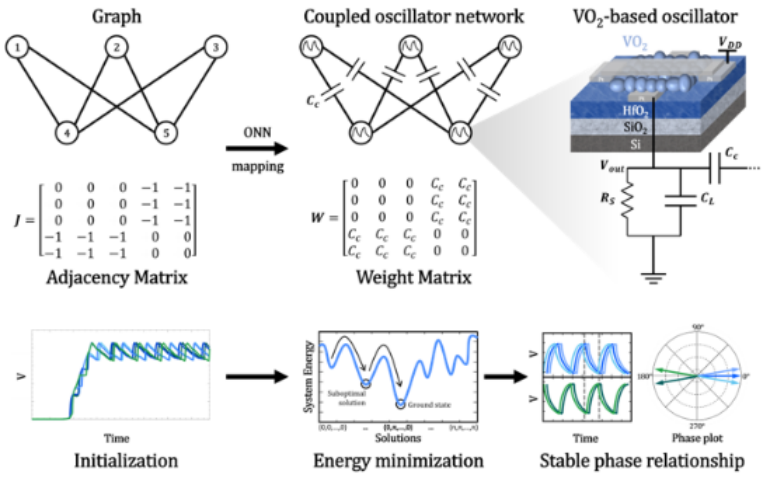

Figure 2.1: From the connected graph to the vanadium dioxide network. Weights are stored in a weight matrix; after initialization of the system, it is driven into ground state where a fixed phase relationship between oscillators is defined. Figure taken from[6]

2.3 Vanadium dioxide-based oscillators

This section is devoted to an overview on oscillator devices based on vanadium dioxide material. As a matter of fact, there exist plenty of different approaches to create an electrical oscillator. RC oscillators are very easy to implement and are suited for low frequency operations (under 1 MHz); LC resonators are quite easy to fabricate and are characterized by higher operating frequency compared to RC ones. On the other side, they are difficult to miniaturize due to the presence of the inductor[5]. CMOS-based ring oscillators represent the state-of-the-art for integration into Oscillating Neural Networks (ONN). This class of devices are fabricated in the Front-end-of-the-line (FEOL) of a Silicon wafer and, for this reason, space problems arise when a large network of oscillators has to be implemented. In other words, to have a large number of interconnected oscillators, we consume a large amount of space on the wafer as in a fully connected ONN, the number of coupling connections increases quadratically with the growth of network size[7]. This means that further space in the FEOL must be reserved for the implementation of the coupling circuit. That is of importance since the larger the ONN, the larger is the number of stable patterns that is possible to retrieve. Considering a network with N neurons, the maximum number M of stable states scales linearly with N and is limited to $M < aN$, with $a = 0.14$[8]. Electrical oscillators can also be realized with phase change materials (PCM), such as vanadium dioxide (VO_2). This class of devices can be fabricated in the back-end-of-the-line (BEOL), solving the space limitation problem and allowing large scale integration. Moreover, the inherent in-memory computing feature allows the network to store the state (e.g. connection weight) inside the device itself, eliminating the need of a bulky external (and necessarily fast) memory with a remarkable gain in terms of computation time, space allocation and power consumption. In the following paragraphs, VO_2-based oscillators are accurately described.

2.3.1 VO_2 as phase change material

Vanadium dioxide is a transition metal oxide that exhibits an electrically induced phase transition close to room temperature (340 K); this property makes it attractive for low power operations. Its insulator-to-metal transition (IMT) is associated with an abrupt change in the electrical conductivity as well as a change in its crystalline structure: during the transition, the material switches from an insulating monoclinic crystalline structure to a metallic rutile tetragonal lattice. In the present work we are interested in a phase switch driven by an electrical signal. However, IMT can also be triggered by other physical stimuli such as thermal, optical or mechanical[9]. The physical mechanism at the basis of the phase change is still a matter of debate in the scientific community. Some researches[10] cite hot

electron injection as the main physical cause while others[11] lean on a resistivity change induced by the generation and annihilation of oxygen vacancies at the grain boundaries of the granular VO_2 structure when a forward and backward bias is applied. Regarding fabrication methods, stoichiometric nanostructured vanadium dioxide can be synthesized with sputtering, Pulsed Laser Deposition (PLD), Atomic Layer Deposition (ALD), sol-gel method, Chemical Vapour Deposition (CVD), electrospinning and hydrothermal method[12]. In the present work, vanadium dioxide relaxation oscillators has been synthesized by ALD method and the details of the process will be given in section 3.1.1. The combined advantages of low temperature switching together with the large change in the electrical conductivity and the large spectrum of fabrication options have made VO_2 attractive for many different applications: voltage-driven electronic switches, field effect transistors, photodetectors, strain and gas sensor to cite some[12].

2.3.2 Coupled VO_2 oscillators

Taking inspiration from natural world, the theory behind the collective synchronization of a large population of coupled oscillators has been scientifically established. The physical nature of the oscillator does not play a role in the frequency synchronization. Indeed, this type of phenomenon can be observed within chemical/biological or mechanical as well as electrical world. An intuitive example of it can be represented by the synchronous flashing of fireflies observed in some South Asian forests: at night, myriad fireflies rest in the trees. Suddenly, several fireflies start emitting flashes of light. Even if initially they flash incoherently, after a short period, the whole swarm flashes in unison[13]. The theory behind this interesting phenomenon sinks its roots in the so called Kuramoto model and, through it, it is possible to demonstrate that an interconnected system made of N oscillators, each having a certain resonance frequency ω_i, will tend to lock in frequency such that the only information describing the network will be the phase difference between each oscillator and a reference one. Obviously, this theory holds up on ideal assumptions such as the equivalency of the coupling strength between oscillator i and j, i.e. $K_{ij} = K_{ji}$ (K represents the coupling strength between oscillator i and j), and the hypothesis that all the oscillators in the network are identical. Once the network is defined we will have phase locking only if the interaction strength between the dynamic elements is sufficiently high; in the case of weak interaction, the oscillations will be incoherent and the devices will ignore each other. As the Kuramoto model is valid independently from the physical nature that triggers the oscillation and the coupling mechanism, it can be considered a valid theoretical background for ONN based on VO_2 relaxation oscillators.

Chapter 3

Methodology used

In this chapter, an excursus over the technological methods and strategies used to obtain the experimental results is presented.

3.1 VO_2 chip fabrication

The present section is devoted to a description of the fabrication steps that I have performed in the BRNC cleanroom to obtain the VO_2 devices. The fabrication starts with a diced wafer that already had the bottom electrode formed and 50 nm non-stoichiometric vanadium dioxide (VO_x) layer deposited. The substrate consists of a silicon wafer with native 2 nm silicon dioxide (SiO_2) on top and a thin layer of 10 nm hafnium dioxide (HfO_2) deposited by Atomic Layer Deposition (ALD). The Hf_2O layer happens to be a fundamental choice used to improve the VO_2 crystallinity property, preserving the switching mechanism in case of short annealing times and improving overall uniformity among devices[6]. Before ALD deposition of the VO_2 layer on Hf_2O, narrow platinum electrodes are evaporated after the desired pattern has been defined. Bottom electrodes represent the terminals from where the output oscillating voltage is extracted and are connected (off-chip) to the external feedback circuit. The following subsections will cover, step by step, the main fabrication methods used to realize the final integrated chip.

3.1.1 Slow Thermal Annealing

As a first step, the 15 mm x 15 mm dice is annealed by Slow Thermal Annealing (STA). This technique is used to convert VO_x into stoichiometric VO_2 which acquires a granular structure. The annealing process takes place in a Pulsed Laser Deposition (PLD) tool where temperature is gradually increased at a rate of 25 °C/min. The nominal setpoint temperature is 520 °C, once that value is reached,

the chip is annealed for 5-10 minutes. Then the temperature gradually decreases with the same rate. An oxygen flow is used to keep a constant pressure of 5 Pa. Note that only the heater temperature is measured, while the actual temperature of the chip is not directly measured (expected to be around 420° C).

3.1.2 VO_2 patterning

The thin film stoichiometric VO_2 layer has to be patterned to obtain the separated devices. The pattern layout was prepared using KLayout software and an electron beam is used to expose the resist and create the desired geometry. First, the adhesion promoter (Surpass 4000) is deposited and, after dehydration, the e-resist (ARN-7520.18) is applied using a spin coating tool. The spinning process consists of two steps: 5 seconds at 500 rpm and then 60 s at 4000 rpm to obtain a resist thickness of 400 nm. Post-apply bake is performed for 5 min at 180 °C to evaporate the solvent, improve the adhesion and chemical stability of the resist. After e-beam exposure the resist is developed in a solution containing 4 parts of AR300-47 and 1 part of water. To realize the final pattern, we have used Inductively Coupled Plasma (ICP) etching and then oxygen plasma cleaning (3 min @400 W) to remove etched residues. The ICP etching step was performed by the BRNC staff.

3.1.3 Top electrodes pattern definition

Oscillators top electrodes are organized such that they are perpendicular to the bottom ones realizing a cross-bar architecture; they are used to drive the supply voltage to each device. Before defining the pattern for the electrodes a double spin coating procedure is needed: two different e-resists are deposited (first ARP-617.06 and later ARP-672.02) each characterized by a different exposure sensitivity. Both resists are spinned with a two steps recipe (5 s at 500 rpm and then 60 s at 4000 rmp). After each resist deposition a bake is performed (5 min at 180 °C). The sample is exposed through the e-beam tool and development in a solution containing MIBK:IPA (Methyl Isobutyl Ketone : Isopropyl Alcohol) 1:2 concludes the process. The e-beam exposure was performed by the BRNC staff.

3.1.4 Metal evaporation

After exposure and resist development, a metal stack is deposited all over the dice. A Physical Vapor Deposition (PVD) tool is used and the metal is evaporated through a focused electron beam deviated on the metal sample by a magnetic field. The stack to be deposited is composed of 5 nm of titanium, used as an adhesion

layer, and 150 nm of platinum that represents the actual top electrode. Since different chips were fabricated, to prevent excessive platinum consumption, the original recipe, used for the last batch, was modified using a reduced amount of platinum (100 nm) and 50 nm of nickel. It is worth mentioning that oxygen cleaning was performed before metal evaporation to ensure better metal adhesion. This choice was justified after experiencing metal delamination during lift-off attributed to an imperfect cleaning of the sample surface right after resist development. To remove metal from unwanted regions, lift-off process in an acetone solution was performed. Eventually, a final oxygen cleaning is carried out to remove residual metal particles. The operation of the metal deposition tool was performed by the BRNC staff.

3.1.5 Wire bonding on Printed Circuit Board (PCB)

The chip is ready to be mounted (glued) on a PCB and wire bonded to the bonding pads that are accessible through low density connectors placed on the two sides of the printed board. The operation with the wire bonding tool was performed by the BRNC staff. The final sample is screwed inside the cryostat with all four connectors bonded to stripe cables that are accessible from the outer through low density cables. Out of 72 total oscillators on the chip, 70 are connected since it is the maximum number of devices that the PCB can host.

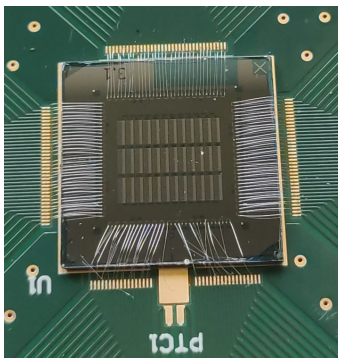

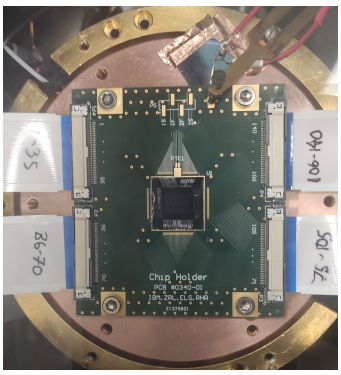

Figure 3.1: Left: An inset of the wire bonded VO_2 chip. Right: Inside the cryostat chamber: PCB mounted on cryostat holder

At this stage, the PCB is ready to be fixed inside the cryostat. The details concerning the experimental apparatus will be given in the next chapter.

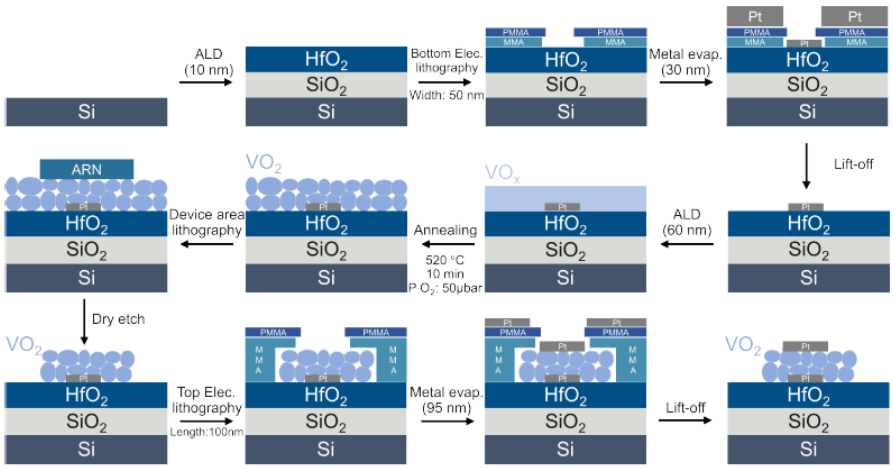

Figure 3.1. Fabrication process of VO_2 crossbar devices.

Figure 3.2: Process flow illustrating steps for the fabrication of the VO_2 chip

3.2 Experimental setup

In this chapter, an overview of the equipment used to conduct and verify the coupling of VO_2 devices is presented.

The desired operating environment is achieved by keeping the wire bonded VO_2 chip inside a cryostat: the PCB is screwed on the holder inside which a constant flow of nitrogen maintains the required operating temperature. Two temperature sensors are installed inside the vacuum chamber: one is used to monitor the temperature inside the holder while the second is kept in contact with the PCB to have more accurate information about the real time temperature at which the oscillators are working.

Two pumps generate Ultra High Vacuum conditions (10^{-8}-10^{-7} mbar) in the chamber: a rafting pump brings the pressure down to 10^{-2} mbar and then a turbo pump is switched on allowing to reach down to 10^{-8} mbar of pressure. On the other side, the temperature is regulated by software and by controlling the refrigerant gas flow through a valve positioned over the nitrogen tank.

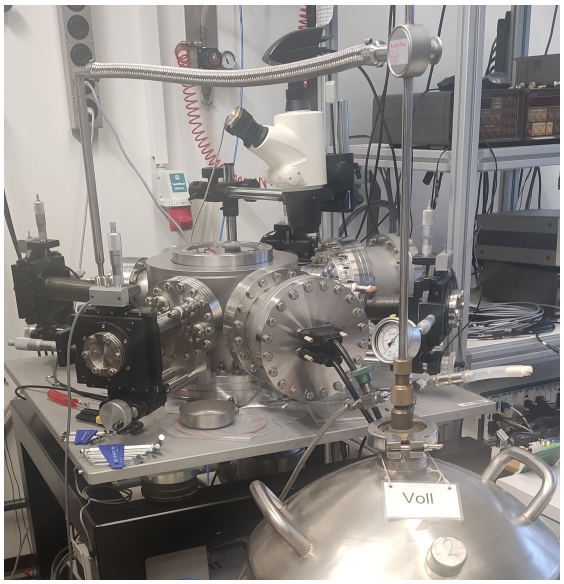

Figure 3.3: Picture showing the cryostat apparatus

All discrete electronic components, used to define the coupling network between the oscillators, are placed on an external breadboard that is connected to the VO_2 chip and to the data acquisition system (DAQ). The DAQ is a National Instrument PXIe-1084 chassis which combines a high-performance 18-slot PXI

Express backplane with a power supply[14].

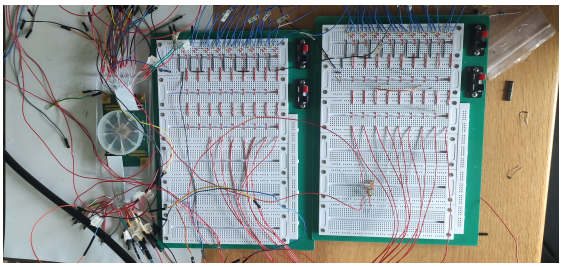

Figure 3.4: Two breadboards where the coupling circuit is implemented

Input and output signals are collected and distributed by the following listed acquisition cards:

- 3 output cards NI PXIe-6738 used to deliver voltage supply/ground signals to the oscillators and to connect them to the breadboard;

- 4 input cards (Pickering and NI PXIe-2727) that define the terminals of series resistances in the feedback circuit;

- 4 input cards NI PXIe-6358 connected to the V_{out} node of each oscillator and used to collect the measured oscillating voltage.

The pinout sequence of the IN/OUT cards can be checked in the official NI website[15]. All the acquisition cards are connected to the NI PXIe-1084 chassis through high/medium density connectors. With the aid of LabView environment, experimental data is collected and visualized. All the parameters are set through the LabView GUI: resistance values in the feedback circuit, supply voltage waveform, voltage amplitude, phase, offset and frequency. Each parameter can be set for each channel that drives one oscillator.

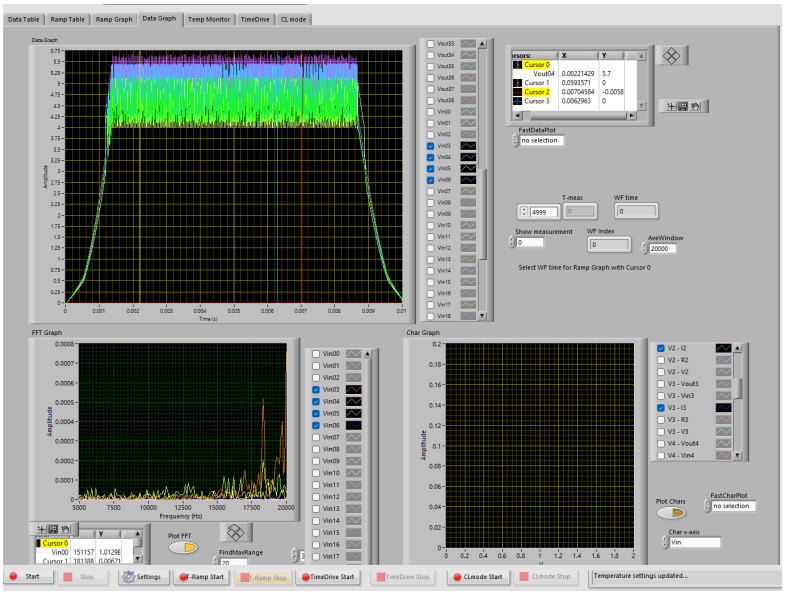

Figure 3.5: LabView output window

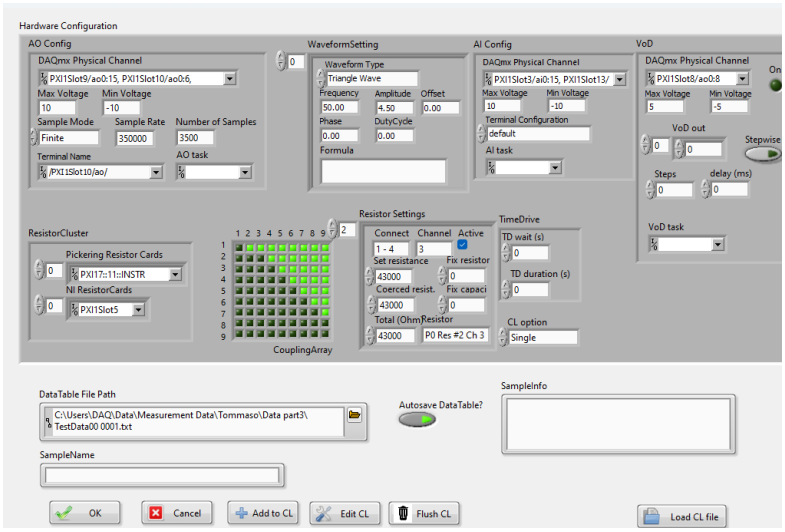

Figure 3.6: LabView control window

Example of experimental test

Once pressure and temperature are set inside the cryostat, the sample is ready to be tested.

- First, a triangular-shape supply voltage with a frequency of 50 Hz and a

typical amplitude of 4-5 V is applied to the oscillators to check which ones are working;

- Once oscillators that work at a reasonable voltage level, with sufficiently large amplitude and stable output wave form are selected, the electrical lumped elements are added to the breadboard to set up the coupling circuit;

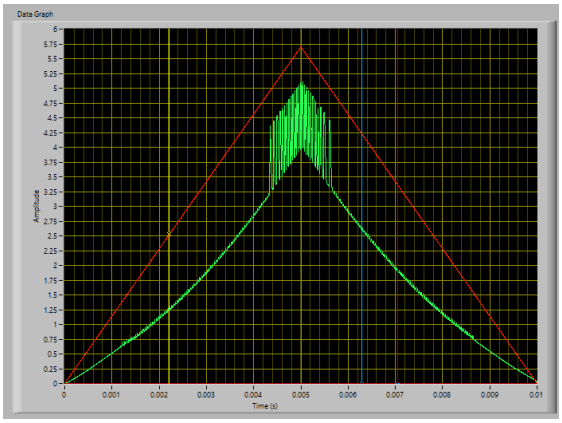

Figure 3.7: Triangular shaped supply voltage (red signal) used to trigger oscillation on a VO_2 device (green signal)

- Supply voltage waveform is switched to a 100 Hz frequency trapezoidal shape pulse to set a time window for the oscillators where we can check the steady-state conditions after the transient. We prefer trapezoidal over square pulses, since a too short falling/raising edge may damage the oscillators;

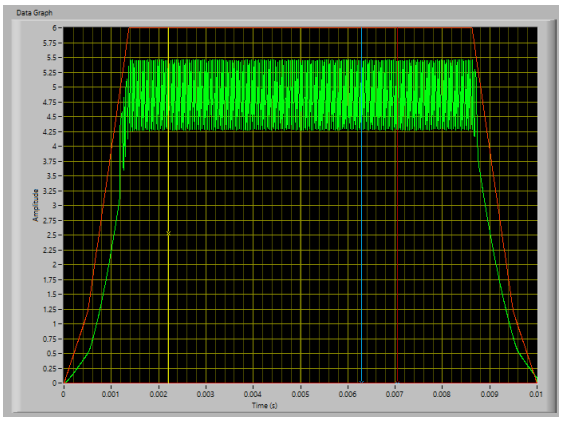

Figure 3.8: Trapezoidal shape supply voltage (red signal) used to drive oscillations (green signal)

- Series resistances with a default value of 40 kΩ are trimmed through LabView software to adjust and align the oscillating frequency of coupled oscillators;
- Multiple tests are carried out until the whole system oscillates at a common resonance frequency, then the established phase relationship between oscillators is checked.

3.3 Coupling schematics

The following section is devoted to the presentation and discussion of the different coupling circuit solutions used later to carry out the electrical measurements, especially the output oscillating voltage of each oscillator of the network.
In the first subsection, a minimal coupling circuit is described comprising only capacitors or resistors . Moving to the next subsections, more complex coupling circuits are presented. In the final part, the integration of the ReRAM chip as a coupling element is fulfilled.

3.3.1 Two coupled oscillators

Capacitive coupling

One simple way to make two oscillators interact is by connecting them through a capacitive element.

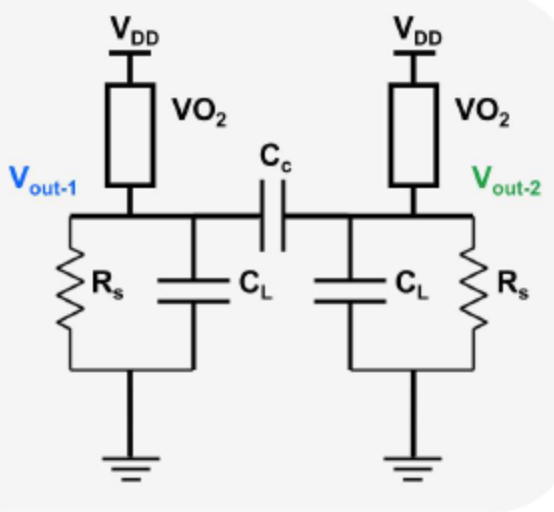

Figure 3.9: Electrical schematic of two capacitively coupled (via capacitance C_c) VO_2 oscillators

Capacitive coupling represents a way to implement negative weights between oscillators. Past experiments have demonstrated the capability of two oscillators to lock in frequency when coupled with a capacitive element[16]. The presence of the capacitor in the coupling circuit has an impact on the circuit dynamics by modifying the effective resonance frequency of the oscillators[16] and allows a dynamic exchange of energy when the supply voltage is driven to the system.

Resistive coupling

As an alternative to capacitors, which may present drawbacks like scalability issues when a large network oscillator has to be implemented, we can use resistive elements in the form, e.g. , of passive discrete resistors. Ideally, resistive coupling justifies instantaneous exchange of energy between connected nodes; indeed, differently from an ideal capacitor, a resistance has a real impedance and thus no phase delay exists between voltage across and current passing through it.

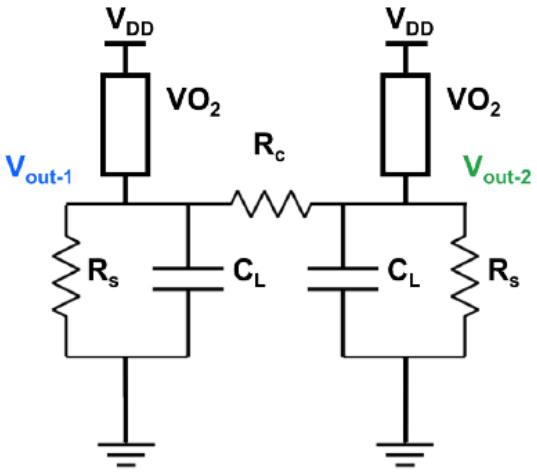

Figure 3.10: Electrical schematic of two resistively coupled (via resistor R_c) VO_2 oscillators

3.3.2 Coupled network of more than two oscillators

Two coupled oscillators represent a basic building block for more complex network of devices and can be used for an in depth study of the oscillation dynamics when circuit parameters are changed (coupling impedance, supply voltage, temperature etc.). However, they are not intended to be used to solve COP for which it is necessary to move to larger networks of interconnected devices. In the present work, Maxcut optimization problem has been investigated with a network of four connected nodes. Using a network of four oscillators for Maxcut optimization can be interesting for multiple reasons: the network is very simple to implement and does not require large number of working oscillators and coupling elements and, at the same time, it can be used to switch between different graph configurations to check for optimization. The image below shows two graph configurations with 4 nodes used as a reference to build small networks of connected oscillators.

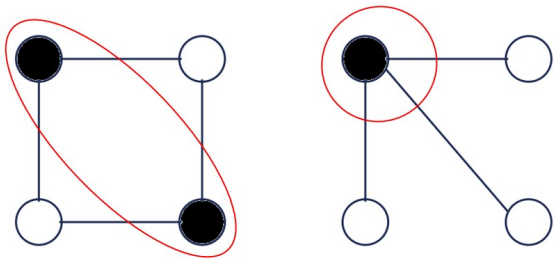

Figure 3.11: Maximum cut optimization for two graphs: nodes are grouped into two partitions (black and white) and the red line shows the cut

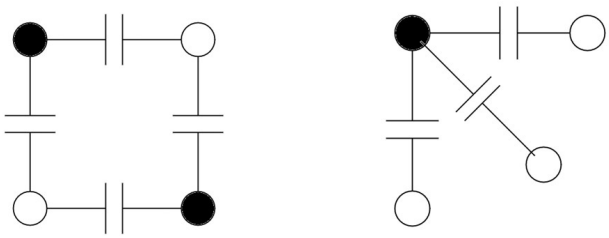

Figure 3.12: Pure capacitive coupling of the connected graphs used for Maxcut optimization

To prepare the field for the integration of a resistive RAM array chip in the coupling circuit, several attempts with discrete electrical elements were performed. In particular, resistive elements used to mimic the RRAM behavior in the high and low resistive states, have been selected as valuable components to implement the desired coupling. As a first test, two different graphs have been realized: they are made of 4 connected oscillators coupled just with a 450 pF capacitor as shown

in figure 3.12. A Second Harmonic Injection Locking (SHIL) signal, capacitively coupled to each oscillator through a 450 pF capacitor, is used to force binarization of the oscillators final state that will result both in phase or 180° out of phase[6]. The same experiments were performed on both graphs, adjusting, time by time, the coupling circuit elements. After measurements of a purely capacitive coupling circuit, a discrete n-type MOSFET transistor is added in series together with a resistance to the capacitor. The intent is to create a dynamic voltage divider represented by the transistor: by acting on the gate voltage it is possible to control the channel conductance and, consequently, the voltage drop across the resistance.

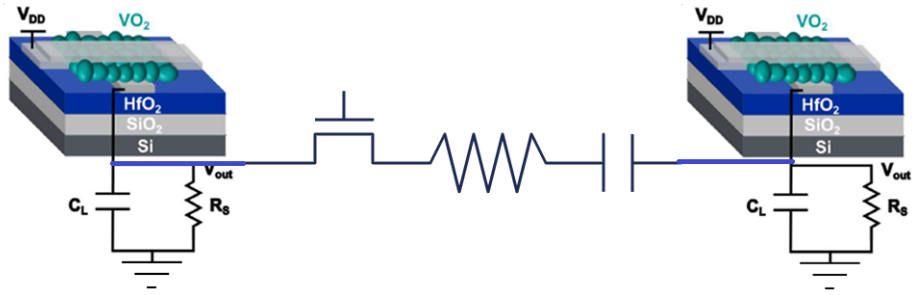

Figure 3.13: Two VO_2 oscillators coupled via a transistor, a resistance and a capacitance

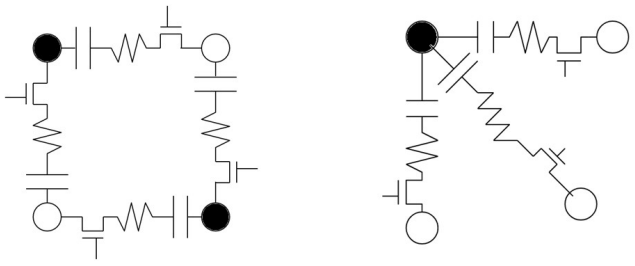

Figure 3.14: Coupling circuit of figure 3.14 applied to the two connected graphs

The following step toward the integration of the RRAM array in the coupling circuit is aimed at assessing the voltage drop across a dummy RRAM, modeled with a standard resistance called R from now on. The use of a resistance to model the RRAM is a rough approximation that does not include the nonlinear behavior of the memristor. To be more precise, the use of R would be fair just to model the RRAM only in the low and high resistive states where it determines whether the interaction strength is respectively strong or weak.
During the oscillation time frame, the current exchanged between the nodes is also oscillating and so is the potential difference at the R terminals. Hence, it becomes of importance to set a maximum voltage drop across R to avoid too large potential difference values that may affect the RRAM state. The voltage drop depends directly on the peak-to-peak amplitude of the VO_2 devices output voltage. A reasonable strategy used to limit this drop is to employ an additional resistance in the coupling circuit (which will be referred as R_c) that acts as a voltage divider for R. The figure 3.15 shows the modified coupling circuit used for this particular test.

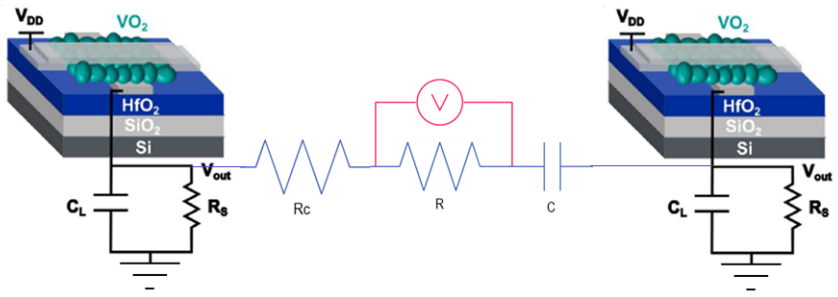

Figure 3.15: Two VO_2 oscillators coupled via a series resistance R_c, a resistance R which models the dummy ReRAM and a capacitance C. In this experiment, the voltage drop across R is measured

A further and final step required the integration of an n-type MOSFET transistor to recreate the dummy 1T1R cell. In this experiment, 4 oscillators are coupled with 5 instead of four connections. This solution has been adopted to realize a kind of graph able to switch between the two configurations just by substituting the value of R without the need to physically remove the connection.

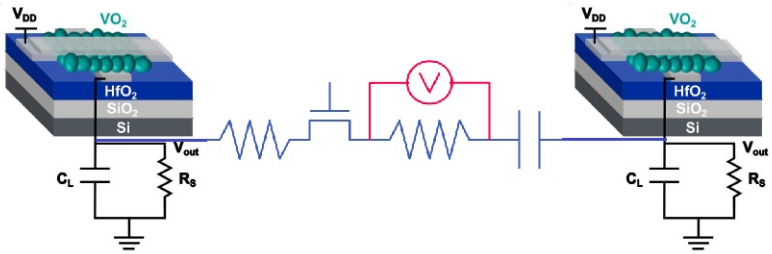

Figure 3.16: Coupling circuit schematic similar to the one presented in figure 3.16 except for the addition of a transistor. Together with R, it models the dummy 1T1R cell

3.4 ReRAM as coupling element

In this section the resistive RAM array is presented. In the first subsection, methodologies used to program the array in the low and high resistive state are discussed, while, in the second subsection, the integration of the RRAM chip in the coupling circuit of the VO_2 network is introduced.

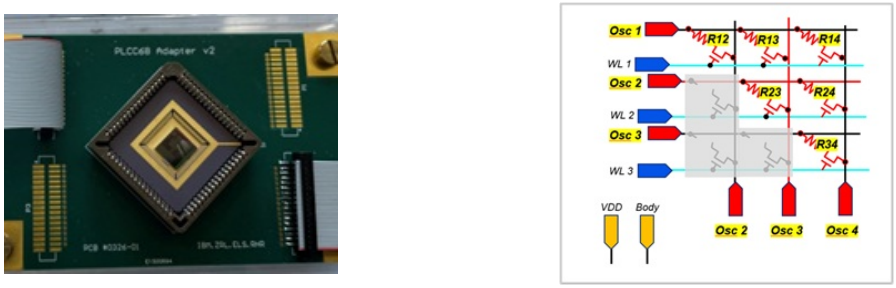

Figure 3.17: Left: 1T1R chip. Right: Schematic of the 1T1R array

3.4.1 Programming ReRAM state

Filament forming

Before starting any operation on the resistive RAM device, it is necessary to apply an initial positive bias to start the so called forming process. This step modifies the structure of the material leading to the creation of a low impedance conductive path between the two electrodes. This conductive path, also called filament, dramatically reduces the resistance of the device, switching it from an insulating state to a metallic behavior. The strong bias applied during the forming process is necessary to induce the migration of oxygen vacancies that form the conductive filament[17]. Once the filament is formed, the device will be enabled to switch between the two states just by acting on the terminal part of the filament.

Set programming

SET operation programs the RRAM in the LRS while it is in the HRS. To perform a SET operation, we use the following procedure:

- The Top Electrode terminal (TE), that corresponds to the Transistor (T) drain node, is strongly biased to bring T into conduction.
- The Gate terminal (G) is biased around 1.4-1.5 V to set the compliance current, i.e. the maximum current allowed to flow in the device preventing permanent breakdown.

The result is that a current smaller than the compliance one will flow in the resistive element generating a low impedance conduction path reducing the resistance of the memristor.

Reset programming

During RESET operation, the device is restored from LRS to HRS. Here are the required steps for RESET:

- TE terminal is grounded.
- Source terminal (S) is positively biased.
- G is biased with a large positive voltage (e.g. 5 V) in order to have the transistor in full conduction.
- This time no compliance current is set.

A current flowing in the opposite direction with respect to the SET case leads to the interruption of the conductive filament at one extremity and, as a result, a transition toward HRS occurs.

3.4.2 ReRAM integration

An array consisting of 8 1T1R wire bonded devices is connected to the breadboard and implements the coupling circuit of a network of 4 VO_2 oscillators. The circuit is completed with 450 pF coupling capacitances and a SHIL signal coupled through a 100 pF capacitance. The 1T1R chip is programmed such that all 8 devices are set in LRS and, in this case, they are prevented from switching to HRS allowing strong coupling between two connected oscillators. In the schematic below are shown the two graph configurations used to optimize Maxcut problem.

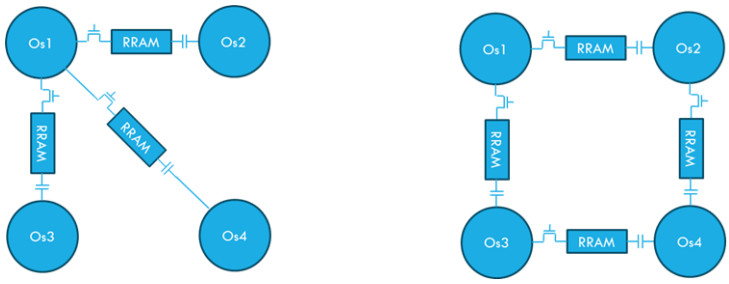

Figure 3.18: Connected graphs with the 1T1R chip integrated in the coupling circuit

3.5 Analog phase tuning

In the previous sections it has been shown how what could be called "digital" coupling between oscillators works, i.e. the phase delay in the time domain can be either zero or half oscillation period (180°). In other words, the coupled oscillators can settle in-phase or in opposition of phase with respect to a reference signal (one oscillating voltage taken as reference) and no intermediate states are allowed. This type of coupling is enforced by the presence of a SHIL signal. A different approach consists of having a tuned phase delay that assumes intermediate states between 0° and 180°; this can be referred to as analog phase tuning.
Using analog phase tuning in an ONN means the possibility of solving different kind of COP where it is required to have more than just two stable states when the system reaches the equilibrium conditions. For instance, it could interesting to be used to solve the 3-SAT or the graph-coloring optimization problems.
The aim of analog phase tuning experiment is to have a fine adjustment of the phase delay depending on the impedance of the coupling circuit. To test this behavior, a small network of two oscillators has been implemented and used to carry out some measurements. The coupling circuit comprises a 100 pF capacitor and a discrete n-type MOS transistor while the controlled parameter is the transistor gate voltage.

3.5.1 Resistive analog phase tuning

Using a transistor to finely tune the coupling strength between the oscillators represents an interesting approach that allows a certain degree of re-programmability just by acting on the gate terminal. Another interesting approach consists in leveraging the multi-LRS or HRS of a resistive RAM to finely tune the phase delay. That is, substituting the transistor with RRAM device. As in the "digital coupling" case, passive resistors of different values are tested in the coupling circuit, together with a series 100 pF coupling capacitance, to mimic the RRAM multi-LR/HRS and to check and measure the resulting phase delay. The need of the capacitance is motivated by the fact that, with low resistance values (which emulates the RRAM LRS), the coupling strength would be so high that oscillators would stop to work remaining fixed in either metallic or insulating state. It also allows some delay in the exchanged current during operation. The results concerning resistive analog phase tuning are shown in section 4.5.1 of the next chapter.

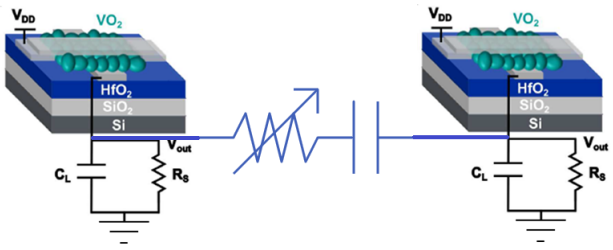

Figure 3.19: Schematic of the coupling circuit used for analog phase tuning experiment

3.6 Spice simulation of coupled oscillators

In order to obtain meaningful experimental results from the VO_2 chip it is necessary to have an integrated device characterized by large yield in terms of working oscillators. The measurement of different coupling circuits involves the constant replacement of discrete components such as resistors, capacitors, MOS transistors and the necessity of wiring all components checking for the correctness of the circuit. For all those reasons, it is worth to have a compact model for the VO_2 oscillator and perform software simulations on different coupling solutions, comparing them with the experimental results. This solution allows for a faster test of the circuit and prevents hand wiring and better re-configurability of the circuit parameters. The software platform used for the simulation is LTSpice and the compact VO_2 model is the one designed by Maffezoni et al.[18]. The figures below show the coupling circuit schematic with two oscillators and the compact model of the VO_2 device.

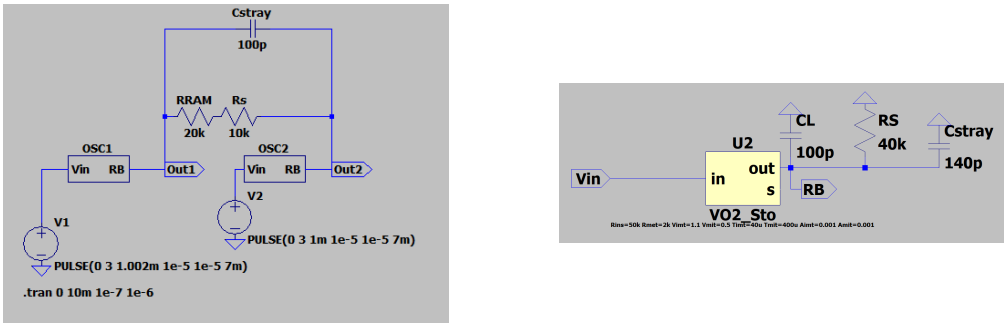

Figure 3.20: Left: Spice screenshot of two coupled VO_2 oscillator. Right: Spice screenshot of a single oscillator (Maffezzoni model in the yellow box) with the feedback circuit

The coupling circuit is made up of two resistances and a 450 pF capacitor. One resistance, named RRAM in the schematic, is used as a dummy resistive RAM in the same way as was used in the real experiment. The second resistance (R_c) acts as a voltage divider to prevent a too large voltage drop at the extremities of RRAM element. A stray capacitance of 100 pF is added between the two oscillators, as well as a parasitic capacitance of 140 pF in the feedback circuit to create an environment which is as close as possible to the measured values in the real experimental setup.

Chapter 4

Experimental outcomes

4.1 Vanadium-dioxide oscillator characteristic

Before diving into the measurements results from the coupling of oscillators, the current-voltage (IV) characteristic for a single VO_2 oscillator is presented. To obtain the graph, a low frequency (10 Hz) triangular sweep supply voltage has been applied. A series resistance of 1 kΩ is connected between the bottom electrode of the oscillator and the ground terminal. The current is measured as the ratio between the voltage drop across the oscillator and the resistance value. The following figure shows the characteristic measured at the temperature of 251° K and 268° K. It highlights a hysteretic behavior between the insulator-to-metal (IMT) and the metal-to-insulator transition (MIT).

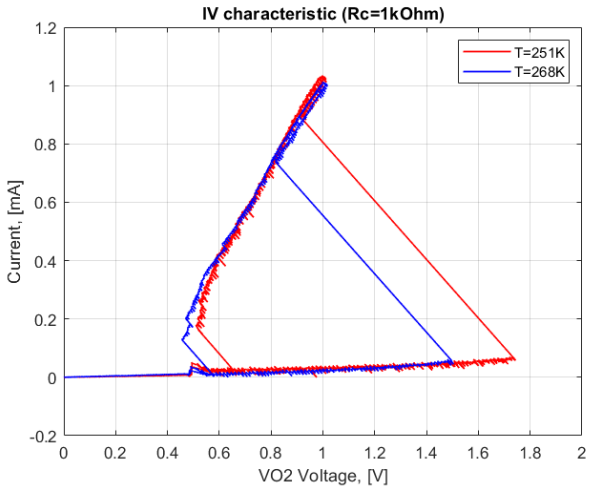

Figure 4.1: Hysteresis curves representing the IV characteristic for a single VO_2 oscillator. Red and blue curves were obtained respectively at 251° K and 268° K

It is possible to observe a fair linear behavior for the device operating in the insulating state. Non linearity in the IV characteristic arise when the device is in the metallic state. The voltage thresholds corresponding to the critical electric fields that trigger the phase switch are altered as we change the temperature. Indeed, at higher temperature, less energy is needed to turn VO_2 into the metallic state, hence the threshold voltage V_{IMT} is reduced with increasing temperature. This behavior can be clearly observed in figure 4.1: at 251° K the switching voltage is between 1.7 and 1.8 V while, just an increase of 17° K in temperature, has the effect of reducing V_{IMT} to less than 1.5 V.

Feedback circuit

The IV characteristic hysteretic behavior becomes a problem for the onset of self-sustained oscillations because the voltage thresholds for MIT and IMT are different and the device tends to remain in one of the two stable states (generally in the insulating state). To settle a fine oscillating behavior between the two equilibrium points, a feedback circuit is needed. For this purpose, we can implement a negative feedback circuit made of a variable resistance or a transistor in series with the VO_2 device[6]. The resistive element generates a load that is translated into a negative differential region on the IV characteristic; the figure below shows a simplified sketch of the IV curve and the intercepts between it and a load line generated by the feedback circuit.

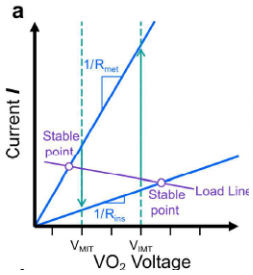

Figure 4.2: Effect of the feedback resistance on the hysteretic IV curve: a load line is generated and it intercepts the characteristic in two points that happen to be the metallic and insulating state of Vanadium dioxide. Figure taken from[6]

This turns the hysteretic behavior of the system into a non-hysteretic one where the transition is favored between the two unstable points resulting from the intercepts between the VO_2 IV characteristic and the load line of the series element[6]. In other words, the presence of the series element creates an instability in the circuit and, if the proper resistance value is selected, the load line slope is adjusted until the output voltage measured across the feedback element starts to switch periodically from a high value, corresponding to the metallic state of the

VO_2, to a low one that coincides with the insulating state and thus a lower voltage drop on the series element. Since the unstable points during oscillations are set by the feedback resistance, it looks reasonable that there exist resistance values for which we have no oscillations at all, i.e. it is possible to define a range of values inside which oscillations are triggered whereas stopped outside of it.

4.2 Capacitive and resistive coupling

The present section is devoted to the presentation of the oscillating voltage outcome measurements of a simple network comprising two oscillators coupled first with only capacitors and then just with resistors. Afterwards, the same measurements are shown for a network of four oscillators coupled with passive discrete components involving a combination of resistors, capacitors and nmos transistors. The network is arranged such that it implements two different graphs for Maxcut optimization.

4.2.1 Purely capacitive coupling

In the figures below are shown graphs relative to the oscillating voltage of two uncoupled and capacitively (through a 450 pF capacitor) coupled oscillators. The present measurements have been performed at 225° K degrees.

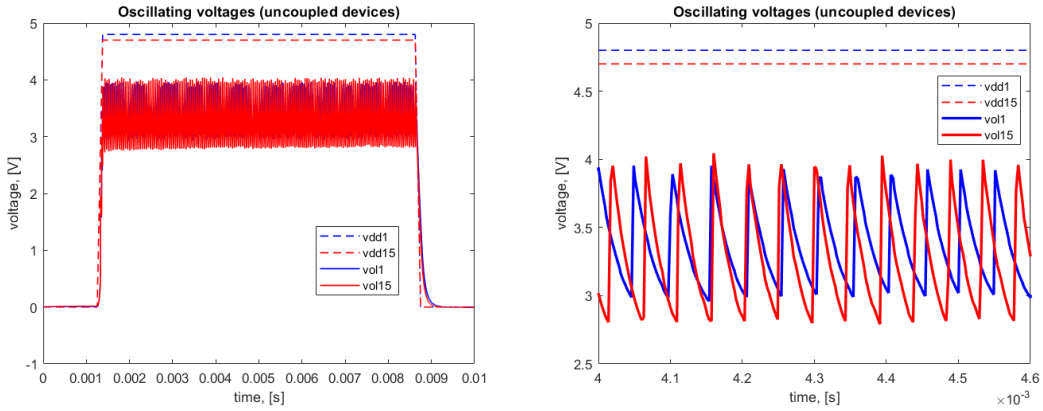

Figure 4.3: Left: Oscillating voltage of two uncoupled oscillators. Right: Inset of the voltage profile, dashed curves are the supply voltages while solid curves represent the output periodic voltages. No frequency synchronization is observed

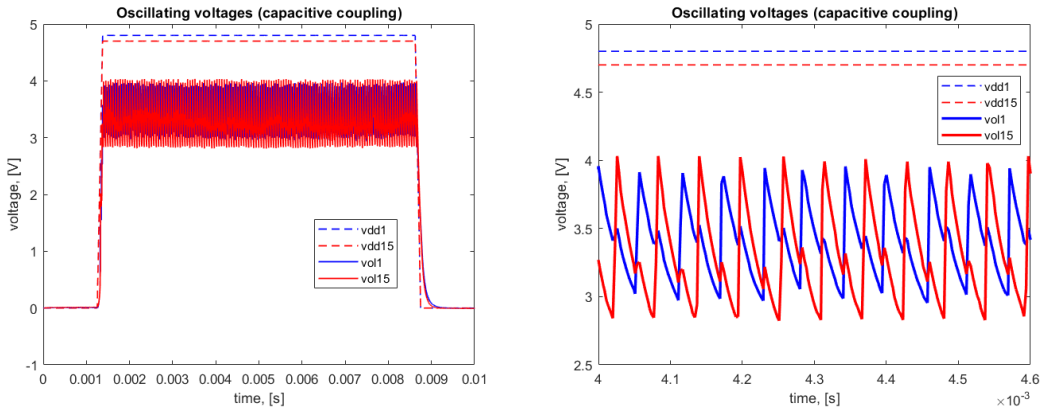

Figure 4.4: Left: Oscillating voltage of two oscillators coupled with a capacitor. Right: Inset of the voltage profile, dashed curves are the supply voltages while solid curves represent the output periodic voltages.

4.2.2 Purely resistive coupling

Experimental results from two oscillators coupled with discrete resistors are shown in the following graphs. The value of the coupling resistance is gradually increased by 10 kΩ starting from 10 kΩ up to 50 kΩ. Going over 50 kΩ will result in a very low interaction strength leading to weakly coupled or uncoupled oscillators. The operating temperature is 250° K.

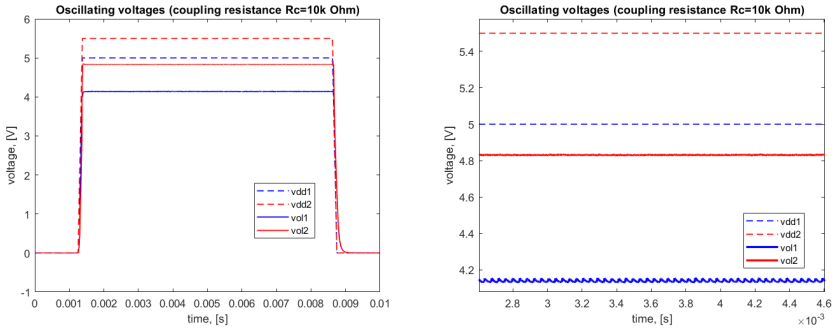

Figure 4.5: Left: Output voltage of two oscillators coupled with a 10 kΩ resistance. Right: Inset of the voltage profile

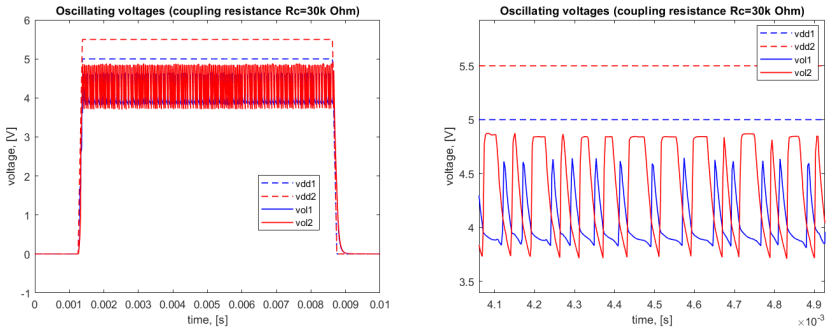

Figure 4.6: Left: Output voltage of two oscillators coupled with a 30 kΩ resistance. Right: Inset of the voltage profile

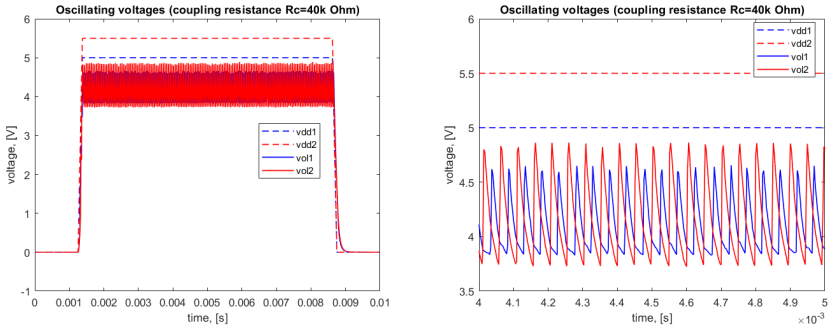

Figure 4.7: Left: Output voltage of two oscillators coupled with a 40 kΩ resistance. Right: Inset of the voltage profile

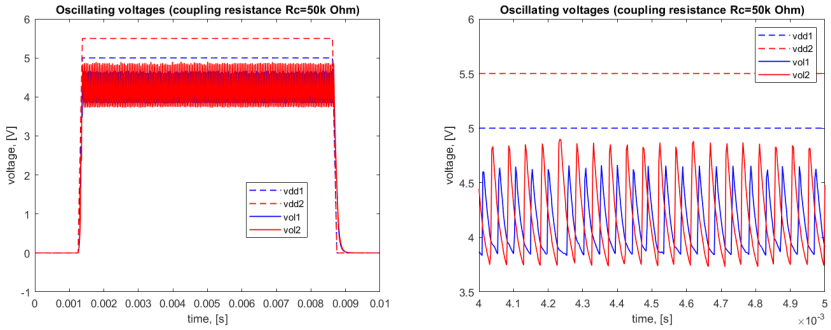

Figure 4.8: Left: Output voltage of two oscillators coupled with a 50 kΩ resistance. Right: Inset of the voltage profile

4.3 Four coupled oscillators network for Maxcut optimization

The following plots show a coupled network of four VO_2 oscillators used to map a graph for Maxcut optimization. All the following measurements were conducted at 250° K. The first two couples of graphs refer to purely capacitive coupling.

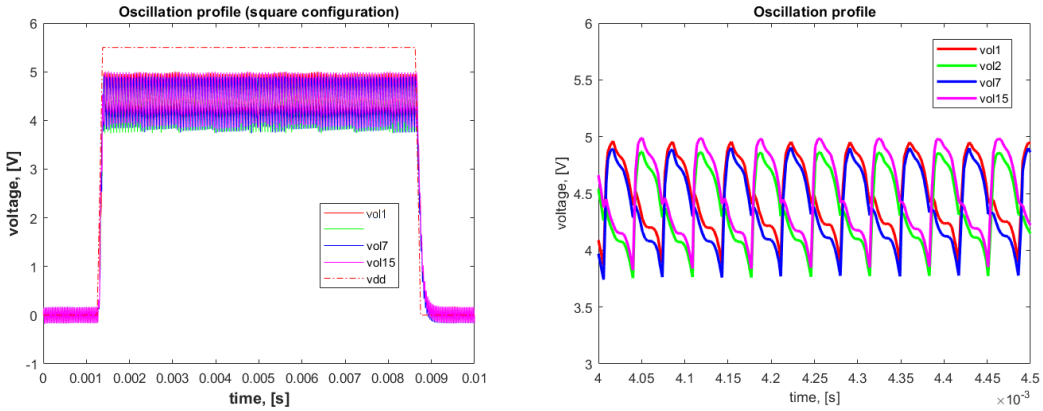

Figure 4.9: Left: Oscillating voltage for the square Maxcut configuration Right: Inset of the voltage profile

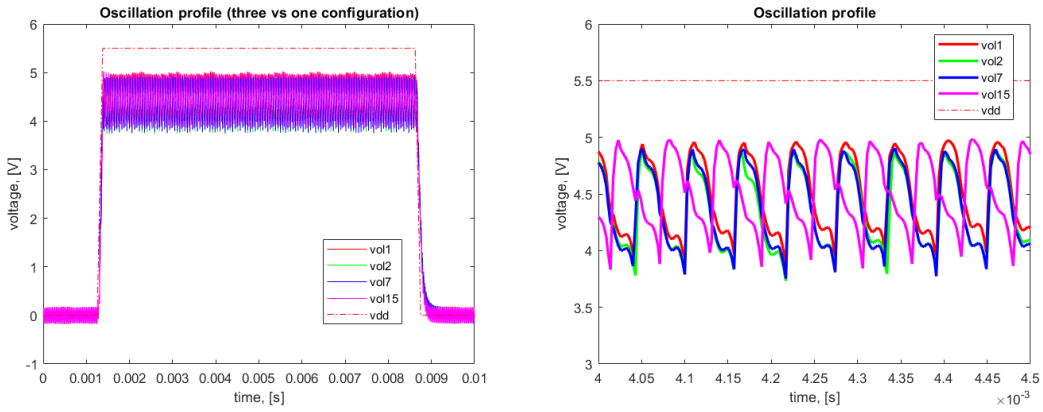

Figure 4.10: Left: Oscillating voltage for the 3 vs 1 Maxcut configuration Right: Inset of the voltage profile

The same measurements are shown below: this time a 10 kΩ resistance and an nmos transistor were added in series as described by the coupling circuit shown in figure 3.13 of section 3.3.2.

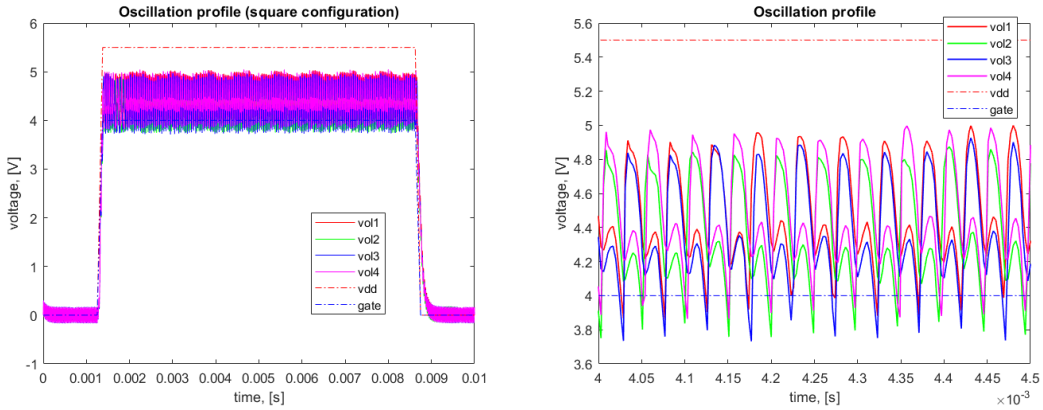

Figure 4.11: Left: Oscillating voltage for the square Maxcut configuration Right: Inset of the voltage profile

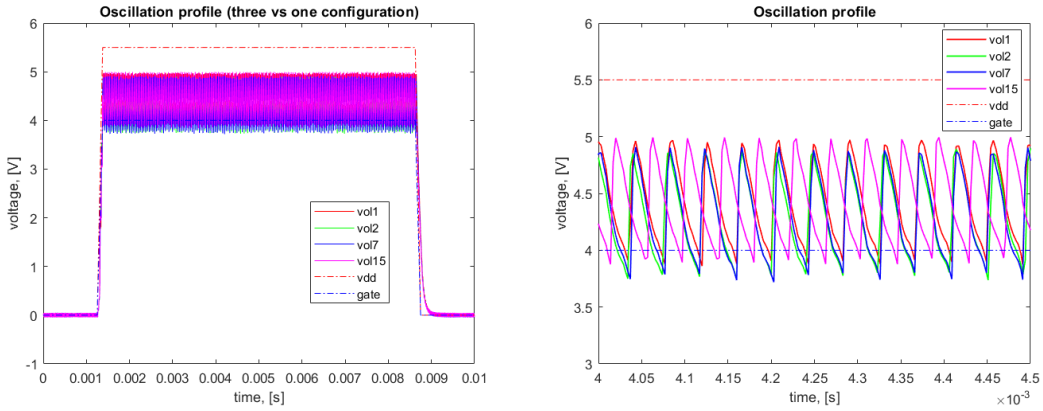

Figure 4.12: Left: Oscillating voltage for the square Maxcut configuration Right: Inset of the voltage profile

The following measurements refer to a network of 4 oscillators coupled through 5 connections. The coupling circuit, resumed in figure 3.16 of section 3.3.2, comprises an 8 kΩ series resistance (R_c), a 450 pF coupling capacitance and a resistance R whose value may be chosen to be 10 k or 100 kΩ representing respectively the states of low/high resistance and thus the strong/weak coupling nature of interaction.

Differently from the previous graphs, here are shown a zoom of the oscillating voltage (on the left) and a plot of the voltage drop measured at the extremities of R (right graphs) to check for safe operating regime. A SHIL signal through 450 pF capacitors was also injected to force a better binarization.

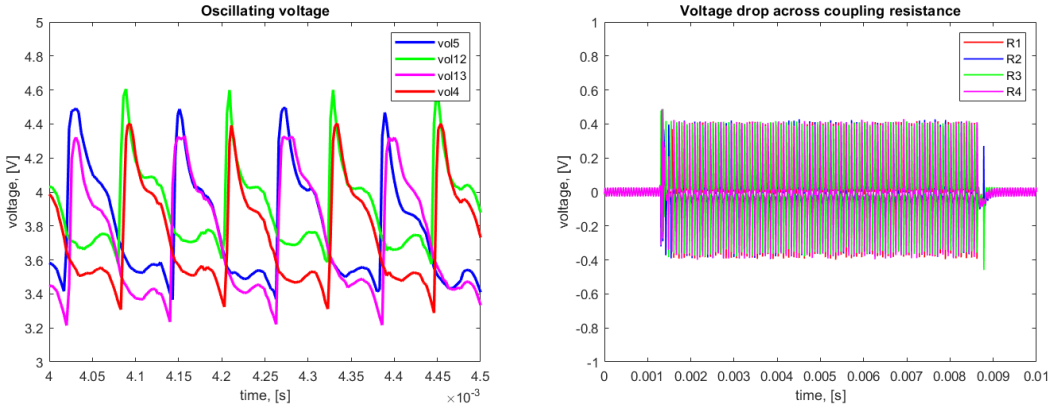

Figure 4.13: Left: A zoom of the oscillating voltage for the square Maxcut configuration Right: Voltage drop measured across coupling resistances R_i with i=1,2,3,4 representing the branch in the graph

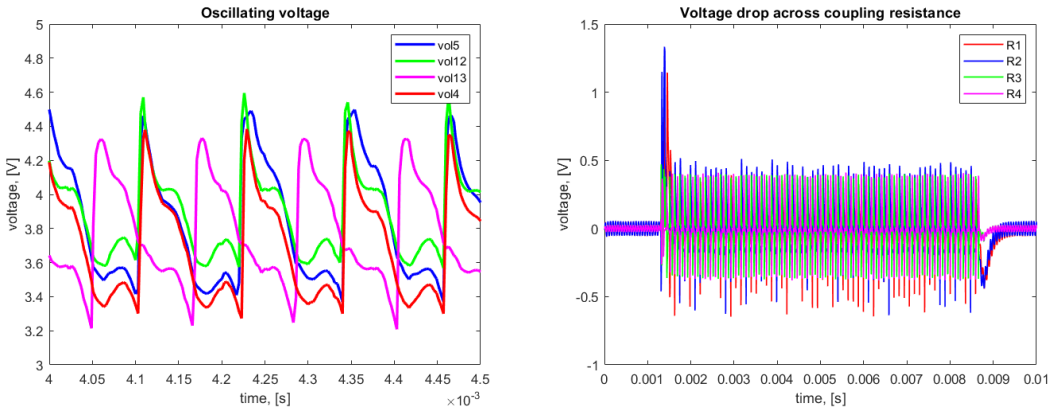

Figure 4.14: Left: A zoom of the oscillating voltage for the 3 vs 1 Maxcut configuration Right: Voltage drop measured across coupling resistances R_i with i=1,2,3,4 representing the branch in the graph

Eventually, the last two pairs of graphs show the same measurements as before but with the addition of an nmos transistor in the coupling circuit which, together with R, mimics the 1T1R cell (the schematic is drawn in figure 3.16).

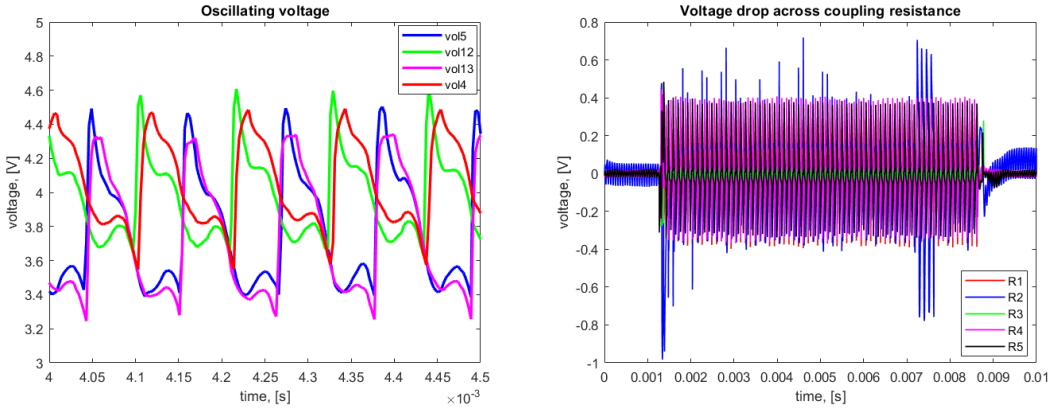

Figure 4.15: Left: A zoom of the oscillating voltage for the square Maxcut configuration Right: Voltage drop measured across coupling resistances R_i with i=1,2,3,4 representing the branch in the graph

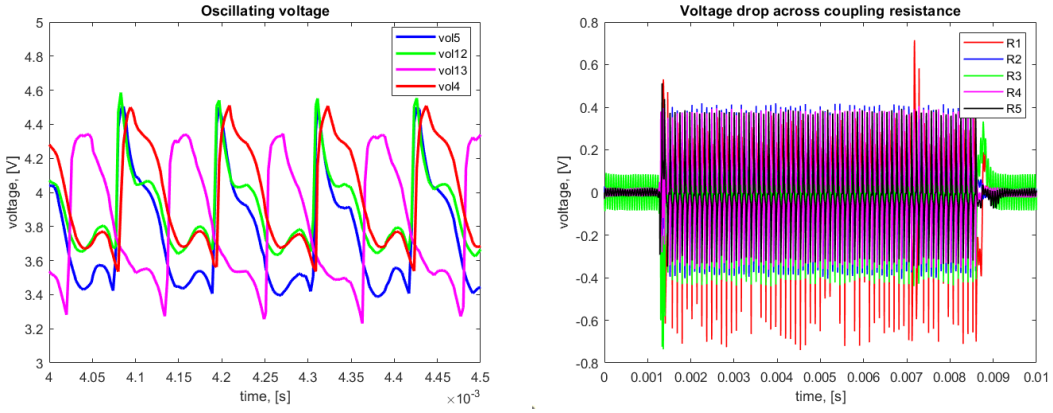

Figure 4.16: Left: A zoom of the oscillating voltage for the 3 vs 1 Maxcut configuration Right: Voltage drop measured across coupling resistances R_i with i=1,2,3,4 representing the branch in the graph

4.4 ReRAM coupling

In the present section, the oscillating voltage plots resulting from the integration of the 1T1R chip in the VO_2 coupling circuit for the optimization of Maxcut problem are shown in the following graphs. The operating temperature is 250° K. The behavior of the system in the frequency domain, shown in the figures 4.17 and 4.18 (on the right), clearly confirms a synchronization of the VO_2 devices with a resonant frequency slightly above 16 kHz. A temporal evolution of the system in steady-state condition is plotted on the left side where it is possible to observe a fully optimization of Maxcut problem for the square (figure 4.17) and for the 3 vs 1 configuration (figure 4.18).

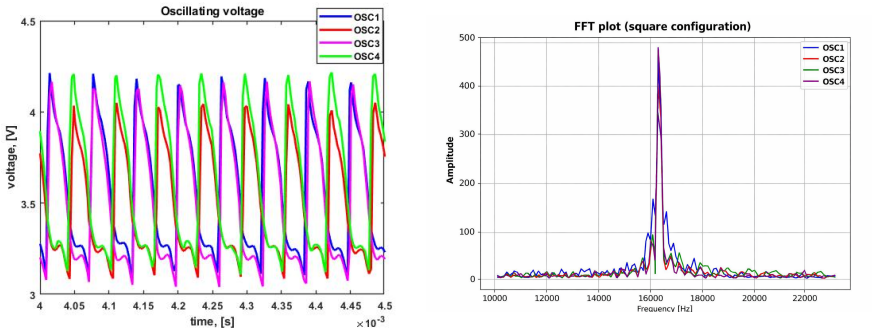

Figure 4.17: Left: A zoom of the oscillating voltage profile of four oscillators coupled in the square configuration. The coupling circuit comprises LRS 1T1R devices. Right: Fast Fourier Transform (FFT) plot of the oscillating system

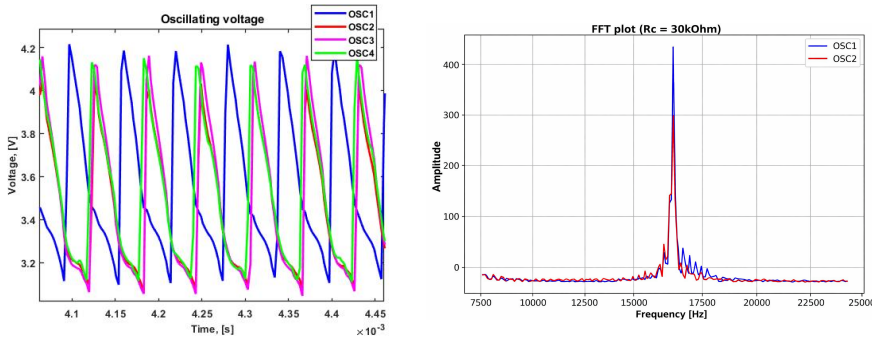

Figure 4.18: Left: A zoom of the oscillating voltage profile of four oscillators coupled in the 3 vs 1 configuration. The coupling circuit comprises LRS 1T1R devices. Right: FFT plot of the oscillating system

4.5 Resistive analog phase tuning

In section 3.5.1 the methodology used to implement the resistive analog phase tuning experiment has been presented and, in the present section, results relative to two oscillators coupled via a RC series circuit are displayed. The resistance value is changed at each experiment to allow different coupling strengths and to observe the relative phase shift effect. The selected range for the coupling resistance lies between 1 kΩ and 30 kΩ; this set of values has been chosen to model a suitable range that is likely to be assumed by the ReRAM chip.

4.5.1 Experimental results

The following graphs refer to voltage measurement from selected resistance values in the coupling circuit. On the left it is possible to observe a the frequency spectrum of the oscillating voltage when the system has reached the equilibrium. On the right, a polar plot of the phase delay was derived by measuring the time difference between two minima of the oscillating voltages and normalizing it with respect to the oscillating period. The period was measured for each oscillation cycle to take into account possible cycle-to-cycle time variability. The final oscillating period, used to normalize the time delay, is obtained as an average over all the periods computed for each oscillation cycle inside the time window when the system has reached stability (i.e. sufficiently far from initial and final transient).

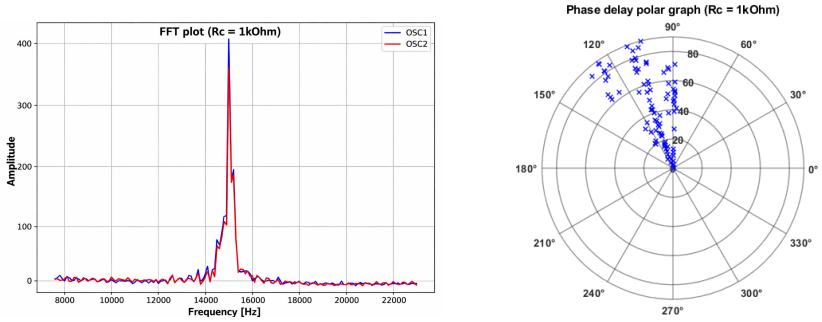

Figure 4.19: Right: FFT plot of the two coupled oscillators with 100 pF capacitor and 1 kΩ resistance. Left: Polar graph which highlights the phase delay between the two oscillators

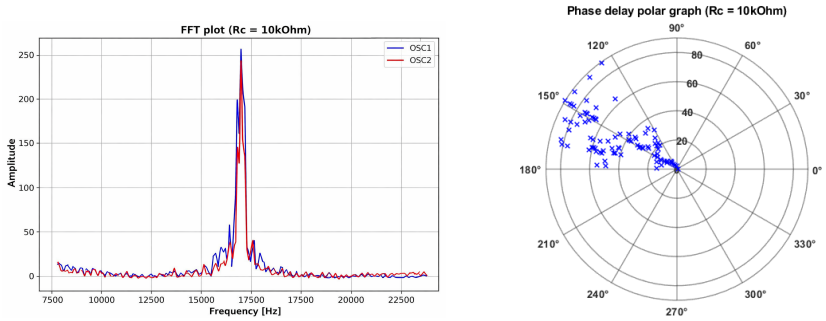

Figure 4.20: Right: FFT plot of the two coupled oscillators with 100 pF capacitor and 10 kΩ resistance. Left: Polar graph which shows the phase delay

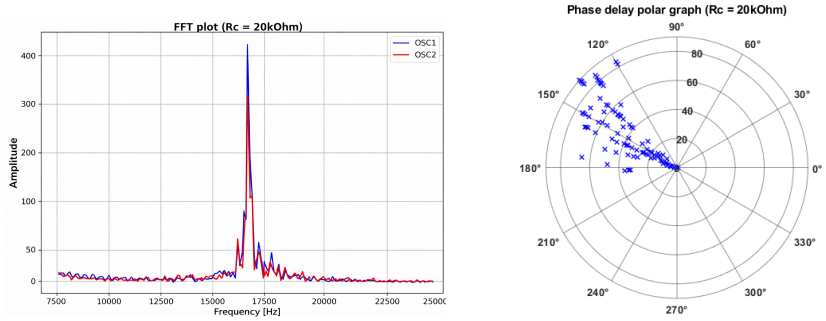

Figure 4.21: Right: FFT plot of the two coupled oscillators with 100 pF capacitor and 20 kΩ resistance. Left: Phase delay polar graph

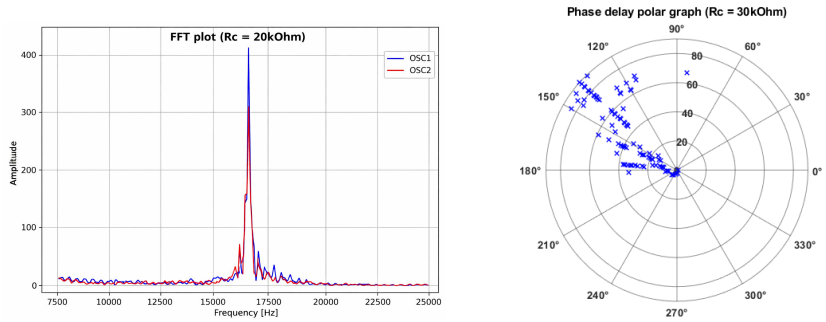

Figure 4.22: Right: FFT plot of the two coupled oscillators with 100 pF capacitor and 30 kΩ resistance. Left: Phase delay polar graph

All of the above illustrated measurements have been conducted at 250° K degrees. The following graphs, presented in figures 4.23 and 4.24, show the condensed results from a sequence of measurements involving multiple values of the coupling resistance (displayed on the x-axis). The experiment has been repeated at different operating temperatures: 225°, 250° and 270° K degrees. The phase delay between the oscillators was measured, at each oscillation period, when the system reached a certain stability after the initial transient. The phase mean value and standard deviation have been stored and plotted for all resistance values used in the coupling circuit.

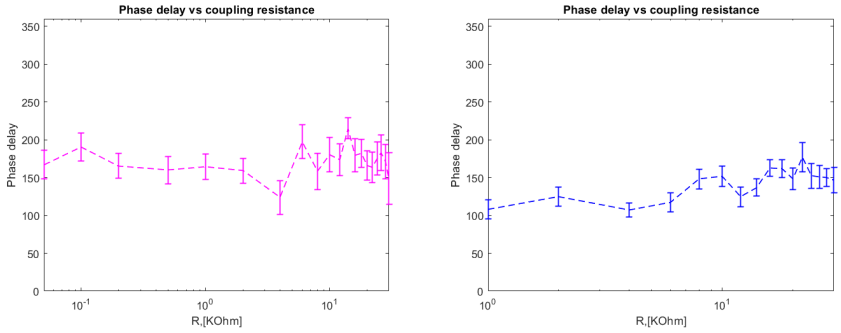

Figure 4.23: Right: Average phase delay with standard deviation measured for each coupling resistance in the specified range on the x-axis. The operating temperature is 225° K. Left: Same graph obtained at the temperature of 250° K

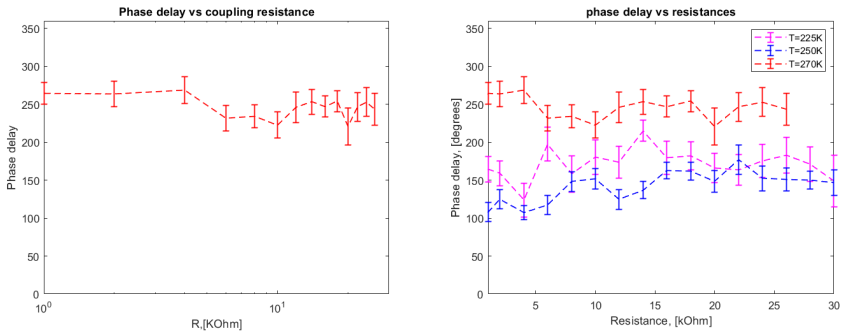

Figure 4.24: Right: Average phase delay with standard deviation measured for each coupling resistance at the operating temperature of 270° K. Left: All previous curves overlapped in the same graph.

4.6 Spice simulation results

Before presenting the simulation of a two oscillator coupled network, it is worth comparing the simulated oscillating waveform, obtained from the VO_2 Maffezoni model, with the real device periodic signal output. The parameters of the compact model are:

- Rins: VO_2 resistance in insulating state
- Rmet: VO_2 resistance in metallic state
- Vimt: voltage threshold corresponding to insulator-to-metal transition
- Vmit: voltage threshold corresponding to metal-to-insulator transition
- Timt: time constant required for IMT
- Tmit: time constant for MIT

Each variable has been appropriately modified to adapt the originally sinusoidal-like waveform in order to resemble an RC charge/discharge profile that better matches the behavior of the real oscillating voltage.

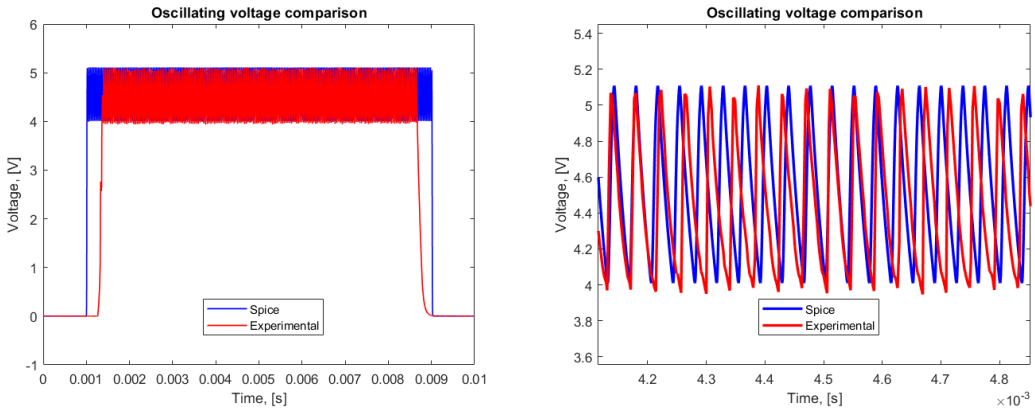

Figure 4.25: Left: Oscillating voltage profile for the Spice model VO_2 device (blue curve) and for the experimental one (red curve). Right: An inset of the oscillating voltage from the figure on the left.

From the right image, it is possible to appreciate the similarities between the two waveforms: rise and falling time of the periodic signals are similar and the voltage amplitude is fairly the same; one main difference is the slight variability in the peak to peak amplitude, which is present in the experimental output and absent

in the simulated curve. This is clearly ascribed to the fact that real oscillators are affected by process variability.
The following graphs present the oscillating voltage outcomes obtained from the simulation of two coupled oscillators.

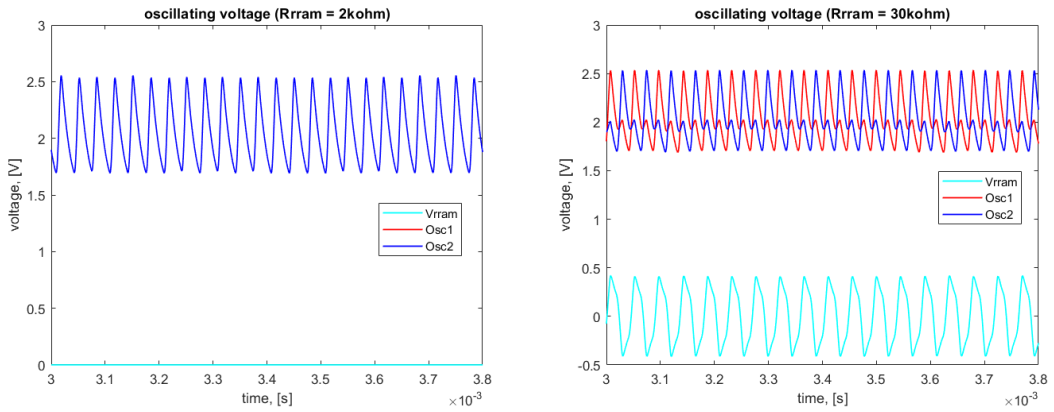

Figure 4.26: Left: In-phase behavior of two coupled oscillators in Spice simulator. The output voltages appear totally overlapped when the coupling resistance is 2 kΩ. The flat light blue curve stands for the voltage drop across the coupling resistance. Right: Out-of-phase coupling of the devices when the coupling resistance is set to 30 kΩ. Below, the voltage drop which is limited in the interval (-0.5,0.5) V.

From the two graphs it is possible to appreciate how frequency locking can be tuned to be in phase or out of phase just by reprogramming the ReRAM resistance value from 2 kΩ, which likely matches the LRS of the real ReRAM, to 30 kΩ, corresponding to HRS. The light blue curve keeps track of the voltage drop across the ReRAM element: it falls to zero when the oscillators have zero phase delay, whilst it oscillates under 0.5 V in absolute value in the out of phase case. This value corresponds to an R_c of 8 kΩ that represents a good compromise in reducing the voltage drop across ReRAM in the HRS and, at the same time, maintaining a sufficiently high difference between strong and weak coupling. The ability to switch from zero to 180° phase delay is lost when the parasitic capacitance value is increased, i.e. the coupling strength is increased. Indeed, the capacitive element will have a bigger impact in the coupling circuit forcing an out-of-phase locking even when the ReRAM element is in the LRS.

Chapter 5

Discussion over results

This chapter is devoted to a discussion of the experimental outcomes presented previously. The order of the following sections is organized so that it follows the same sequence proposed for the previous chapter, that is, the results are discussed in the same disposition as they were shown in the experimental part.

5.1 Two coupled oscillators

5.1.1 Capacitive coupling

The measurements results relative to two capacitively coupled VO_2 devices clearly show that the oscillators lock in frequency and their phase delay is about 180°. That result is coherent with theoretical expectations since the ground state, which corresponds to the minimization of the energy Hamiltonian, is obtained when the spins in the Ising Hamiltonian equation (section 2.2.2) have antiferromagnetic behavior with a negative coupling, that is, the voltage levels between oscillators should be opposite: when one oscillator is in the metallic, the other one is in the insulating state and vice versa. To explain the phenomenon in a different way, the presence of the capacitance introduces a delay in the exchange of energy between the oscillating nodes and pushes out-of-phase the connected oscillators.

5.1.2 Resistive coupling

When two Vanadium dioxide devices are coupled resistively, the oscillating voltage profile, measured after ground state is reached, points out the inability of our oscillators to lock in frequency in the in-phase configuration. It is well known that positive coupling, achieved through purely resistive elements, allows oscillating nodes to synchronize together reaching ground state with zero degree of phase delay between them. This has been shown in experimental work by Corti et al.[19]

where, depending on the value of the coupling strength, i.e., the resistance value, a system of two coupled VO_2 devices stabilizes either in-phase (strong coupling with low resistance value) or in opposition of phase (weak coupling with high resistance value). Concerning the graphs measurements presented in section 4.2.2, we can draw some conclusions based on the value of the resistance. When the coupling resistance value is 10 kΩ, the interaction strength is so high that the current exchanged blocks any chance for oscillators to jump again from one state to the other. Basically, we have one device trapped in the metallic and the other in the insulating state. Lowering the coupling strength, e.g moving to 20-30 kΩ of coupling resistance, we can observe some oscillation attempts even if the waveform quality is not sufficient to be used for valuable problem optimization experiments. Moving to 40-50 kΩ values, nice oscillations with stable behavior and sharp wave profile are favored. At these values of resistance, the exchanged current is fairly high to allow easy frequency synchronization (by tuning the series resistance in the VO_2 feedback circuit) and, at the same time, at a level that prevents oscillations from blocking. As we further increase the resistance value, we enter in a weak coupling regime and the exchanged current levels are not sufficient to allow phase locking; in other words, oscillators can be considered as uncoupled ignoring each other and oscillating at their own resonance frequency. Independently from the resistance value, as stated at the beginning of this section, the 2-coupled oscillators system is unable to lock with an in-phase behavior. To give an exhaustive explanation of why the expected phase configuration was not experienced would require further experiments; however, the non negligible stray capacitance between neighbor oscillators, could play a crucial role in pushing the devices out-of-phase. Indeed, we can model the actual coupling circuit not as a purely resistive one but with the addition of a parallel capacitance which leads to a complex coupling impedance and adds a delay between exchanged current. Once reduced the entity of the parasitic capacitance by acting on the experimental setup, could be of interest exploring different resistance values from the one used in our experiment to check for an in-phase locking. In this case, it is important to select relatively low resistances in order to enforce the resistive nature of the connection by avoiding parasitic elements which are always present. At the same time, a too low value would result in no oscillations at all, hence the range for which the system works in-phase might be very small.

5.2 Maxcut problem optimization through different coupling schemes

Capacitive coupling

The experimental measurements over a network of 4 oscillators used to map a basic Maxcut problem graph are displayed in sections 4.2 and 4.3. The first discussed experiment involves a capacitor as a coupling element. For the first graph, each pair of oscillators in the diagonal happen to be in phase while there are three oscillators in phase in the second configuration. By grouping in one subpart of the graph all the oscillators that are in phase, it is possible to determine the graph maximum cut equal to 4 in the square configuration and 3 in the three vs one configuration. This proves that a capacitive element tends to push out-of-phase connected oscillators. In phase coupling can be observed between uncoupled or weakly coupled oscillators and could be interpreted as an indirect effect resulting from out of phase alignment, i.e. weakly coupled oscillators appear to be in-phase just as a consequence of being pushed away by the neighbor nodes with whom the interaction is strong. It is of relevance to act on the SHIL amplitude: a too small amplitude does not binarize correctly the system, with a phase delay between oscillators comprised between zero and 180°; instead, an excessively large amplitude, might force the oscillator resonating at double the frequency or even damaging it, resulting in no more oscillations.

Mixed resistive-capacitive coupling

When a more complex coupling circuit is introduced in the oscillatory system, multiple attempts for the optimization of the Maxcut problem are needed. Indeed, also the energy landscape of the oscillatory network becomes more complex and the chances of being trapped in a local minimum with a failure in the optimization of the COP are higher. By finely tuning the feedback resistances, changing the coupling circuit parameters and the SHIL amplitude, it was possible to obtain acceptable results in terms of Maxcut optimization. Looking at figures 4.13 and 4.14 on the left, the phase-locking of the output voltage confirms a cut of 4 for the square configuration and 3 for the 3 vs 1 design. On the right, plots of the voltage drop across the resistances R, used to mimic the RRAM device, point out a safe limit under 0.5 V (in absolute value) which would avoid the re-programming of the RRAM element. However, it is important to notice a large spike above 1 V in the initial transient in figure 4.14 left. This is caused by a slight delay in the initial switching on of the oscillators and could be reduced by adjusting the supply voltage signals time delay such that all the oscillators are turned on at the same time. To further complicate the coupling circuit, a nmos transistor was introduced

and used to emulate the T element in the 1T1R cell. Clearly, this adds a further degree of complexity which reduces the chance to get the optimal solution for the connected graph. The elevated degree of instability can be checked in the zoom of the oscillating voltages (figures 4.15 and 4.16 on the left), where the green and red curves, representing two uncoupled oscillators, can be considered in-phase, as a first approximation, even if a small delay between them exists. Nevertheless, optimization of Maxcut problem is achieved in the same way as it was obtained in the previous experiment. The voltage drop, measured at the ends of the series of the transistor and the resistance R, i.e. the whole 1T1R element, is displayed on the left graphs. Overall, we can assess a safe voltage drop below 0.4 V for the majority of the oscillation cycles. Small spikes above 0.8 V are present and are associated with the sudden instability of the circuit which does not maintain a fixed phase relationship over the whole operating time window. It is worth to mention that, in order to optimize the afore described coupling circuit, an important tradeoff has to be taken into account: reducing the voltage drop across the 1T1R element when R is in the HRS is fundamental and requires an increase in the value of the series resistance R_c; on the other hand, a high value of R_c in the connections where there is a low R value, will obviously hinder the high coupling strength dictated by R, and so it will affect the coupling ratio (reducing it) between strong and weak coupled connections. This might affect the optimization of the graph. For this reason, a compromise in the selection of the coupling circuit parameters is required.

ReRAM integration in the coupling circuit

One remarkable result concerning Maxcut optimization consists in the integration of the resistive RAM array in the coupling circuit of a 4 VO_2 oscillators network. The ground state oscillating voltage that corresponds to the optimum cut for a specific graph has been shown in the figures 4.17 and 4.18 of section 4.3. From the first graph, related to the square graph configuration, as the steady-state condition, corresponding to synchronized and stable over time oscillations, is reached, the oscillators located on the opposite sites of the graph happen to be in-phase and out-of-phase with respect to neighboring ones. As confirmed from previous experiments, a maximum cut of 4 is obtained. A similar conclusion can be drawn for the result on the three vs one graph configuration. After some transient cycles, the system reaches ground state and thus stable oscillations within the time window of the trapezoidal-shape supply voltage. Oscillator number 4, which is the only one connected to all the other devices, is out of phase with the other three devices. The cut for this graph is 3 and corresponds to the maximum. The presented results clearly suggest that the RRAM device programmed in the LRS behaves as a resistance of roughly 2kΩ and provides the desired strong interaction between connected oscillators.

5.3 Analog phase tuning

A preliminary analysis on the experimental results regarding analog phase tuning shows that the ability to control the phase delay by means of the coupling strength intensity is characterized by high randomness. Looking at the phase mean value as a function of the coupling strength, independently from the temperature at which we are taking the measurements, it is evident the fact that no clear monotonic trend in the phase relationship can be extracted when the coupling resistance is increased. On the other hand, a visible phase dependency on the operating temperature can be deduced: working at lower temperatures pushes the two oscillators around a configuration which is more out-of-phase while, as we move to higher temperatures (270° K), the phase delay is, on average, around 250° K. A larger number of experiments would be needed to confirm whether this behavior is reproducible or simply the result of a random process. It is interesting to observe a superior stability in the phase delay, in terms of smaller standard deviation, if we look at the measurements taken at 250° K with respect to the same at 270° K. This could be an indication of higher stability for the network of connected oscillators as temperature is lowered.

Obviously, using a temperature controller to drive phase tuning is not energetically and time efficient and, as said before, several repeated experiments would be needed to assess if such a control can be reproduced with a certain degree of reliability. The inability to fine control the phase delay acting on the coupling resistance could have multiple origins. A non negligible influence on the oscillators state may come from crosstalk with neighboring devices which are weakly coupled through a parasitic capacitance. In this sense a re-arrangement of the chip design or simply a change in the measurement setup may help reducing parasitic elements and relative energy exchange between ideally uncoupled devices. It also could be possible to have a wrong selection for the set of tested resistances: we have chosen a quite broad range going from 1 kΩ up to 30 k Ω inside which we have selected about 15 resistances and, based on the observations done on successful analog phase tuning by means of a coupling transistor, there could exist a smaller range of conductivity values for which analog tuning can be possible and so a narrower set of resistances inside the (1 kΩ - 30 k Ω) range. A valuable approach might consist in measuring the channel resistance of the transistor, working as a coupling element between the VO_2 couple, and substitute it with a tunable resistor (ideally a multi-LRS ReRAM) which assumes the same resistance values.

Chapter 6

Summary

Resistive switching devices and in particular, as the main actor for the present thesis, vanadium dioxide-based relaxation oscillators, represent an alternative yet valuable candidate as a building block to realize ONNs suited for next generation computing architectures. This work has focused on different approaches regarding the coupling of VO_2 units, starting from simpler solution involving passive discrete components, to more complex circuits where several parameters had to be optimized in order to get the desired results. Passive circuit elements such as resistor, capacitor and transistors, had served to model the 1T1R cell containing a ReRAM device which, due to its inherent re programming ability and in-memory capability, represents the ultimate approach to implement connections between the oscillators in order to store directly in the device the coupling strength, i.e the synaptic weight between the artificial oscillating neurons. The VO_2 chip, hosting up to 70 oscillators, was fabricated in the BRNC cleanrooms and then stored for the experiments in a cryostat at UHV conditions and relatively low temperature (around 250° K). The coupling circuit was implemented off chip through hard wiring of the electronic components on an external breadboard. To prove the correct functioning of the coupling circuit, small network containing four coupled oscillators were tested to optimize Maximum-cut COP with different connected graphs. The most meaningful experimental outcomes shown the correct optimization of Maxcut graph using a resistance, a nmos transistor and a capacitance as coupling circuit (reproducing the 1T1R cell) together with a series resistance which sets an acceptable voltage drop across the dummy ReRAM. After phase synchronization of the oscillators (in-phase or out-of-phase), by looking at the steady-state oscillating voltage profile and grouping on the same sub partition the devices (nodes of the graph) with same phase, it was possible to check whether or not the obtained ground state was the one corresponding to the maximum number of cuts for the specified graph. Additionally, the full 1T1R chip containing 4 LRS ReRAM devices was integrated in the coupling circuit showing the correct optimization of Maxcut problem. Eventually, analog

phase tuning was tested using a minimum network of two VO_2 elements connected via a capacitance and a resistance with tunable value. The experimental results does not prove a fine phase control by means of the coupling resistance value but rather a quite random behavior of the phase relationship which seems more temperature driven.

Bibliography

[1] «https://en.wikipedia.org/wiki/Decision$_p$*roblem*». In: () (cit. on p. 3).

[2] «https://en.wikipedia.org/wiki/Combinatorial$_o$*ptimization*». In: () (cit. on p. 3).

[3] Olivier Maher et al. «A CMOS-compatible oscillation-based VO2 Ising machine solver». In: *Nature Communications* 15.1 (2024), p. 3334 (cit. on p. 3).

[4] «https://en.wikipedia.org/wiki/Maximum$_c$*ut*». In: () (cit. on p. 3).

[5] Yi Zhang et al. «Oscillator-network-based ising machine». In: *micromachines* 13.7 (2022), p. 1016 (cit. on pp. 4, 5).

[6] Olivier Maher. «Solving Complex Optimization Problems with Neuromorphic VO-based Oscillators». In: (2025) (cit. on pp. 4, 7, 19, 28).

[7] Wooseok Choi et al. «Hardware implementation of ring oscillator networks coupled by BEOL integrated ReRAM for associative memory tasks». In: *2025 IEEE International Memory Workshop (IMW)*. IEEE. 2025, pp. 1–4 (cit. on p. 5).

[8] Elisabetta Corti. «Networks of Coupled VO2 Oscillators for Neuromorphic Computing». PhD thesis. EPFL, 2021, p. 28 (cit. on p. 5).

[9] Suman Datta, Nikhil Shukla, Matthew Cotter, Abhinav Parihar, and Arijit Raychowdhury. «Neuro inspired computing with coupled relaxation oscillators». In: *Proceedings of the 51st Annual Design Automation Conference*. 2014, pp. 1–6 (cit. on p. 5).

[10] K Appavoo, NF Brady, M Seo, J Nag, RP Prasankumar, DJ Hilton, and RF Haglund. «Ultrafast phase transition in vanadium dioxide driven by hot-electron injection». In: *EPJ Web of Conferences*. Vol. 41. EDP Sciences. 2013, p. 03026 (cit. on p. 5).

[11] Wanheng Lu, Lai-Mun Wong, Shijie Wang, and Kaiyang Zeng. «Local phenomena at grain boundaries: An alternative approach to grasp the role of oxygen vacancies in metallization of VO2». In: *Journal of Materiomics* 4.4 (2018), pp. 360–367 (cit. on p. 6).

[12] Yanqing Zhang, Weiming Xiong, Weijin Chen, and Yue Zheng. «Recent progress on vanadium dioxide nanostructures and devices: Fabrication, properties, applications and perspectives». In: *Nanomaterials* 11.2 (2021), p. 338 (cit. on p. 6).

[13] Juan A Acebrón, Luis L Bonilla, Conrad J Pérez Vicente, Félix Ritort, and Renato Spigler. «The Kuramoto model: A simple paradigm for synchronization phenomena». In: *Reviews of modern physics* 77.1 (2005), pp. 137–185 (cit. on p. 6).

[14] «https://www.farnell.com/datasheets/3750682.pdf». In: () (cit. on p. 12).

[15] «https://www.ni.com/docs/en-US/bundle/pxie-6358-specs/page/specs.html». In: () (cit. on p. 12).

[16] Nikhil Shukla et al. «Synchronized charge oscillations in correlated electron systems». In: *Scientific reports* 4.1 (2014), p. 4964 (cit. on p. 16).

[17] Elisa Zaccaria. «Low Temperature Modeling and Characterization of Analog ReRAM for Deep Neural Network Acceleration». In: (2024) (cit. on p. 22).

[18] Paolo Maffezzoni, Luca Daniel, Nikhil Shukla, Suman Datta, and Arijit Raychowdhury. «Modeling and simulation of vanadium dioxide relaxation oscillators». In: *IEEE Transactions on Circuits and Systems I: Regular Papers* 62.9 (2015), pp. 2207–2215 (cit. on p. 26).

[19] Elisabetta Corti, Bernd Gotsmann, Kirsten Moselund, Igor Stolichnov, Adrian Ionescu, Guofang Zhong, John Robertson, and Siegfried Karg. «VO 2 oscillators coupling for neuromorphic computation». In: *2019 Joint International EUROSOI Workshop and International Conference on Ultimate Integration on Silicon (EUROSOI-ULIS)*. IEEE. 2019, pp. 1–4 (cit. on p. 43).